MASTER EN ASTROFÍSICA

COSMIC VOIDS IN THE UP-COMING J-PAS SURVEY: PROSPECTS FOR CMB CROSS-CORRELATION MEASUREMENTS

Autora:

Gisela Cristina Camacho Ciurana

Supervisor:

Andras Kovács

Instituo de Astrofísica de Canarias

Trabajo fin de máster

Curso Académico 2021/2022

Contents

Abstract

Los vacíos cósmicos son las estructuras más grandes y menos densas de la red cósmica. Debido a su peculiaridad y a su sensibilidad a la cosmología, han sido definidos como una poderosa herramienta cosmológica, ya sea por sí mismos o en combinación con el estudio de otros observables cosmológicos. Su huella en los mapas de temperatura y potencial proyectada del fondo cósmico de microondas (CMB) nos permitirán explorar la naturaleza de la energía oscura y los modelos de la gravedad modificada. El estudio de estas regiones es reciente y aún se conoce muy poco sobre ellas. Los ambiciosos cartografiados actuales y futuros de la estructura a gran escala del universo (Euclid, J-PAS, eBOSS, LSST) brindan una oportunidad singular para medir la respuesta de diversos observables cosmológicos y luego confrontar esas medidas con predicciones teóricas. Tales cartografiados permitirán extraer catálogos de vacíos con muestras de trazadores más densas y en épocas más tempranas que las accedidas hasta el momento. Además, es esencial realizar investigaciones sobre los vacíos a partir de las simulaciones y, debido a que sus propiedades los hacen menos sensibles a los efectos de la materia bariónica, pueden ser estudiados usando simulaciones de N-cuerpos de halos de materia oscura, en lugar de usar simulaciones hidrodinámicas completas.

Teniendo todo esto en mente, nos hemos focalizado en simular el poder observacional que tendrá uno de los futuros cartografiados, J-PAS (Javalambre Physics of the Accelerating Universe Astrophysical) survey, correlacionando los vacíos cósmicos a alto redshift, usando quásares a $0.8 < z < 2.2$ como trazadores, con diferentes mapas del fondo cósmico de microondas: Integrated Sachs-Wolfe (ISW), Sunyaev-Zeldovich (SZ) y lentes gravitaciones (κ).

Hemos escogido el futuro J-PAS survey por su combinación de fotometría y espectroscopia en la toma de datos. Nos ofrecerá mucha más densidad de datos de galaxias con menos precisión en su distancia, pero este error en la distancia no es de gran importancia para el estudio de los vacíos cósmicos. Hemos simulado de forma aproximada los datos de QSOs que observará J-PAS survey, cogiendo como base el catálogo de quásares de eBOSS survey, ya que son los únicos datos observacionales de QSOs a alto redshift disponibles actualmente. Luego hemos incrementado en dos pasos, J-PAS low ($1.5x$eBOSS) y J-PAS high ($2x$eBOSS), la densidad de QSOs, para modelar de forma aproximada el incremento en densidad de J-PAS survey ya que se espera que sus observaciones sean más profundas que las de eBOSS survey. Con este fin, hemos usado el catálogo de halos de materia oscura de las simulaciones de Websky, para poblar los halos con QSOs mediante la metodología de *Halo Occupation Distribution (HOD)*. Después, para encontrar los vacíos cósmicos en los catálogos de quásares, hemos usado el algoritmo *2D void finder* [32]. Este código, creado para tratar con redshifts fotométricos, proyecta los QSOs en cortes 2D de redshift (100 Mpc/h) y encuentra en cada uno de estos los centros y los radios (R_v) de cada vacío. El tamaño y el número de vacíos depende principalmente de dos parámetros libres: *smoothing scale* (σ) y *underdensity threshold* (δ_{min}). Para un valor más alto (bajo) de σ encontramos más (menos) vacíos y un valor más bajo (alto) de δ_{min} implica un mayor (menor) número de vacíos cósmicos. Para estudiar la señal de las lentes gravitacionales de los vacíos, hemos escogido el mapa CMB de las simulaciones de Websky y lo hemos correlacionado con la posición de cada uno de los vacíos implementando la metodología de *stacking*. Esta consiste en recortar parches del mapa del CMB alineados con los vacíos cósmicos, y con un re-escalado calcula la señal media, reduciendo así el ruido de los datos. Además, hemos aplicado un *smoothing* Gaussiano a escalas pequeñas (FWHM=1°) y hemos eliminado los modos de gran escala del mapa de κ CMB, para suavizar y limpiar el mapa. Por último, para calcular la señal-ruido (S/N) de κ procedente de los vacíos, hemos realizado 1000 simulaciones aleatorias usando la suma del mapa de ruido aleatorio de Planck [48] y las fluctuaciones de nuestra señal.

Al estudiar la señal de cada mapa del CMB de los vacíos, las lentes gravitaciones del CMB mostraron una mayor señal y menores fluctuaciones, debido a que entre $2 < z < 3$ la señal de κ es

más eficiente. Por esta razón en este proyecto únicamente se estudiará en profundidad la señal de κ en los vacíos cósmicos.

La combinación de parámetros, aplicados al *2D void finder*, que encuentra el mayor numero de vacíos posibles con la mayor señal es $\sigma = 30$ Mpc/h y $\delta_{min} = -0.3$ para los tres catálogos simulados. Aplicando este ajuste de parámetros, hemos calculado la señal de κ y la S/N. J-PAS high presenta la mayor $S/N = 7.1$, aumentando en un 20% la S/N de eBOSS y además, la señal de κ en el interior de los vacíos en J-PAS high es más fuerte (más negativa) en comparación con los otros dos catálogos. Aunque hay una disminución notable en el numero de vacíos a medida que aumenta el numero de densidad de quásares de todo el cielo; para J-PAS high es $N_{voids} = 37449$, mientras que para eBOSS es $N_{voids} = 45818$, encontrándose J-PAS low entre los dos con $N_{voids} = 40641$. Esta reducción del numero de vacíos cósmicos cuando aumentamos la densidad de trazadores (QSOs), se deben a la eliminación de vacíos espurios, los cuales son regiones aleatorias del cielo que el algoritmo los define como vacíos los cuales introducen ruido en los datos. Estos resultados refuerzan la hipótesis de que J-PAS survey mejorará las observaciones realizadas de eBOSS para los vacíos cósmicos. Además, nos informan que J-PAS survey nos permitirá realizar estudios prometedores en cosmología, ya que el catalogo J-PAS high es una estimación conservadora de lo que realmente producirá J-PAS survey.

En el estudio realizado hasta ahora no hemos tenido en cuenta el error del redshift fotométrico en el catálogo de quásares de J-PAS survey ($\sigma_z \sim 0.002(1+z)$). Si lo consideramos para J-PAS high, los resultados muestran una reducción de 10% en el numero de vacíos con una S/N=7.4 y una señal de κ ligeramente más fuerte. Una posible explicación para al aumento de la señal es que los 500 vacíos perdidos son vacíos espurios que desaparecieron tras perturbar ligeramente las posiciones de los QSOs. Finalmente, hemos analizado el efecto en el perfil de κ si aumentamos el redshift. Únicamente hemos encontrado vacíos cósmicos robustos hasta $z = 2.8$ porque a redshifts más altos los quásares están más dispersos. El número de vacíos encontrados en $2.2 < z < 2.8$ supera en un 35% a J-PAS high, contribuyendo a un aumento de la S/N=7.4, pero la señal de κ disminuye. Esto muestra una reconstrucción de los vacíos mala porque los QSOs están muy dispersos.

1 Introduction

This Chapter explores the current knowledge about cosmic voids and their relevance to cosmology. In Section 1.1, we introduce the actual cosmology model, giving an historical overview and a short description of the structure of the Universe at large scales. In Section 1.2, we explain the importance of using cosmic voids as cosmological probes. Section 1.3 we provide a description of the current and future galaxy surveys, explaining in detail the J-PAS survey. Moreover, we make an overview of the actual simulations to study galaxy clusters and cosmic voids. Finally, in Section 1.5, we give a detailed description of the objectives of this work.

1.1 Cosmology and large-scale structure of the Universe

Cosmology is the science that studies the Universe as a whole, with the objective to understand the origin and the evolution of the large-scales structures. This branch covers a multitude of very different fields: from particle physics and its unification models to observations of galaxies in the local Universe of globular clusters in our Galaxy, all within the framework of general relativity. This theory, published by Albert Einstein in the years 1915s and 1916s [1], proposed that gravity is a distortion of the space-time, and is the current description of gravitation in modern physics.

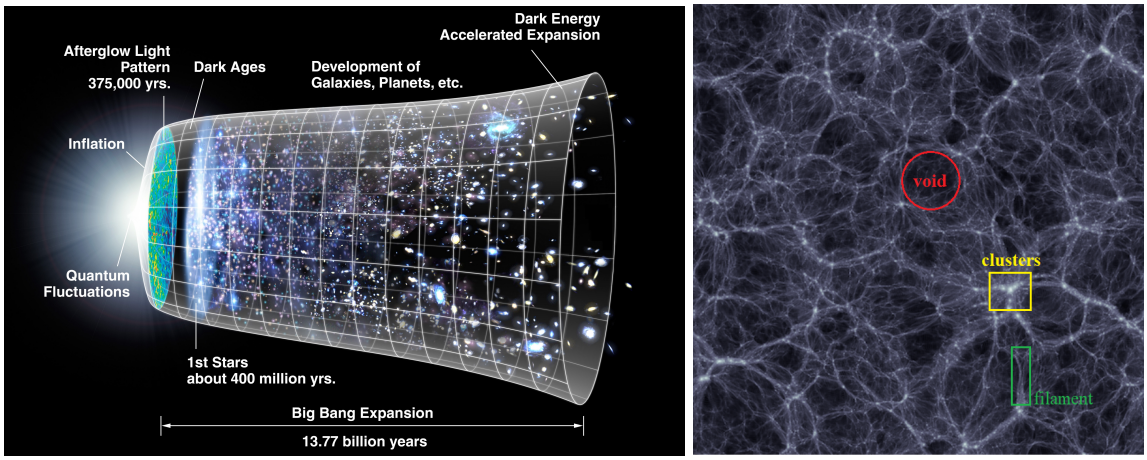

(a) (b)

Figure 1: (a) Representation of the evolution of the Universe over 13.77 billion years. The far left represents the period of "inflation" produced a burst of exponential growth. Then the expansion of the Universe gradually slowed down as the matter is pulled on itself via gravity. At $z < 1.5$ the expansion has began to be accelerated because the effect of the dark energy have come to dominate (Image by Nasa). (b) The Large Scale Structure (LSS) of the Universe, patters of galaxies and matter on megaparsec scales, showing the different components of the Cosmic Web: galaxy clusters, walls, filaments and cosmic voids.

Assuming that this theory was correct on cosmological scales, and also with the information from observations of the large scales structures of the Universe, the theory of the Big Bang was developed. But, it was not until 1965 when Arno Penzias and Robert Wilson measured the Cosmic Microwave Background [11], which confirmed a key prediction of the Big Bang theory and strongly established this model. From that point on, it has been generally accepted that the Universe started in a hot, dense state and has been expanding over time (see Figure 1a).

In 1998, two independent investigations ([7],[9]) found that the Universe was not only expanding, but also this expansion was accelerated, becoming the Λ Cold Dark Matter (ΛCDM) the leading model until now. This model defines the composition of the universe with three main components: dark energy (68%), cold dark matter (27%) and baryonic matter ($< 1\%$). The dark energy is defined by the cosmological constant (Λ), and it causes the accelerated expansion, but its nature is still unknown. And the Cold Dark Matter particles interact with each other only through gravity, and it has not been detected yet.

Furthermore, ΛCDM model provides good account of different properties of the Universe: the existence of the CMB, the abundance of the baryonic matter, the accelerated expansion and the large scale structures. In this project we used the flat ΛCDM cosmological model with the parameters: (Ω_m, Ω_b, h)=(0.31,0.049,0.68), consistent with Planck Collaboration 2018 [12].

On megaparsec scales the matter distribution of the Universe is not uniform, but it forms an intricate and complex spatial pattern which is known as the Cosmic Web [13]. Its structure is due to the gravitational instabilities from the small density fluctuations in the Early Universe throughout the cosmological history. This scenario is favoured by observational evidences and confirmed by present-day large galaxy surveys such as 2dFGRS [14], Sloan Digital Sky Survey (SDSS) [17] and the 2MASS redshift survey [19]. This structure consists of elongated filaments and walls, that surround large and nearly empty *cosmic voids*. At the nodes of the web, there are dense and compact clusters, agglomerates that have thousands of galaxies (see Figure 1b).

Despite the successes of the ΛCDM model of cosmology has gone during all the 21st century and its continued support by some more detailed observations of different phenomena, there is a still poor understanding of the nature of the largest components at a fundamental level. There are possible cracks on including the Hubble tension concerning the expansion rate or, experiments of the weak gravitational lensing calculating the S_8 tension in the context of the current clumpiness structure [10]. Therefore, due to the anomalies with the model, it is important to look for alternatives, as the modified theories of gravity. This theories are centering in explain where the gravity has not been tested accurately: at large distances and scales where gravity is really strong. Moreover, there are non-standard cosmological probes to extract more information from the same data sets, and cosmic voids are part of it.

1.2 Cosmic voids as cosmological probes

Voids are the large under-dense structures that occupy the vast majority of space in the cosmic web and also are promising laboratories for extracting cosmological information. While most of the work to understand the Universe has been focused on the over-dense regions, lately there has been an increase in the interest towards these empty regions.

Our knowledge of the Universe is far from being complete, and cosmic voids are good cosmological probes, since they can help us to have a better comprehension of important matters such as the nature of dark energy, the growth rate of structures, the modified gravity, the sum of neutrino masses or galaxy formations:

- Cosmic voids are *dominated by dark energy*, becoming a new passage to study its nature, because of the lack of matter inside them. They offer a new opportunity to *understand the accelerated expansion* of the Universe, apart from using the high density regions, like galaxy clusters ([28],[29]).

- Studying the matter density profile, along with the shape and the evolution of cosmic voids, allows us to obtain information about the *growth rate structure*. In order to achieve this, one possibility is to use the redshift-space distortion (RSD), which is sensitive to the growth rate.

The use of cosmic voids implies *more simplicity*, because they are non-virialized regions and are dominated by coherent motions [3]. The measurement of the growth rate is a cosmological probe, a key to test the nature of gravity [2].

- Given their intrinsic nature, voids have evolved less, preserving a better memory of the initial conditions, a phenomenon that does not occur in crowded regions. As a result, their study has the potential to connect large-scale structures at late times to the *Early Universe* physics. Besides, Einstein's general relativity deviates more in low-density regions, which enables us to find an alternative theory of gravity ([32],[6]) and primordial non-Gaussianity.

- Cosmic voids can help to put bounds in the mass of neutrinos because, contrarily to the standard model of particle physics, neutrinos do have mass. Due to the lack of matter inside of these regions, voids are *sensitive to neutrinos* [21], their mass fraction is higher than in crowded environmental. By studying the properties of voids, the properties of neutrinos can be found.

- Galaxies in cosmic voids represent a unique laboratory, containing *isolated systems* whose evolution has been driven almost completely by in-situ processes. If it is considered that most of the void galaxies are evolving like an isolate system, this gives the opportunity to study the evolution of a galaxy with no interaction with its environment [22].

To understand cosmic voids in a theoretical framework, the main objective is to be able to model the types of voids that are identified in the real data from galaxy surveys and simulations, due to the fact that it still exists a gap of knowledge between the evolution of individual voids through simulations/observations vs. theory. It is necessary to improve the density and velocity profiles around voids, the void size function and the two-point statistics of voids, in order to gain a better analytical understanding.

1.3 Simulations and galaxy surveys

Cosmic voids are only recently being explored because of the lack of information. Void science has not reached its fully potential as of today, because to do a great study the following ingredients are needed: a large volume, to promise small error bars, large tracer density, to have a detailed mapping of the under-dense structure, and depth fields in magnitude, to reach information about weak and high redshift sources.

There are existing deep simulations that focus on the reconstruction and evolution of the large scale Universe using only galaxy formation, such as SIMBA [25] and the Illustring TNG project [24]. They capture cosmological scales of tens to hundreds of comoving mega-parsecs while simultaneously resolving the internal structure of individual galaxies at $\leq 1kpc$ scales. Large-scale cosmological N-body simulations focused on halo catalogs and the overall cosmic web of dark matter can be done much faster than high-resolution galaxy formation simulations. And because cosmic voids are low density environments, that makes them less sensitive to baryonic effects, and also occupy a large volume of the cosmic web, enable the use of this faster simulations to do a great study. Furthermore, when measuring cosmological parameters with void-related observables we need to understand their degeneracies. For example, the void size function is affected by both properties of dark energy and neutrinos, and RDSs are sensitive to modifications of gravity and neutrinos. Therefore, to fully exploit the potential of voids it is necessary to understand and reduce these degeneracies, and one possibility is to combine voids with other cosmological probes such as galaxy clusters and the CMB secondary anisotropies. For this reason, large volumes are needed to get sufficient statistics to reduce the sample variance.

Together with the simulations challenge, the study of cosmic voids using observations is essential. At this moment, the low redshift voids have already been studied by the Dark Energy Survey (DES) ([42] ,[23]) and the Sloan Digital Sky Survey [8] (SDSS) with photometric redshift data. Moreover, there are on-going surveys, such as the Dark Energy Spectroscopic Instrument (DESI), that will soon provide new observational constraints on the properties of voids [34]. Whereas high-z voids are harder to find, there are only some existing preliminary results from eBOSS. The void science with not just eBOSS (extended-BOSS) but BOSS as well, has been the biggest source of information about voids using spectroscopy. Using eBOSS data in [15], the authors found the void BAO measurements on quasars, concluding that voids can be potentially useful to further increase the BAO detection. Some catalogs of cosmic voids have also been created with eBOSS data to study the growth of the structure around them [16]. These studies conclude that the reconstruction of the cosmic voids can be contaminated because the QSOs catalog do not have a sufficient density, and with the future surveys can be greatly improve.

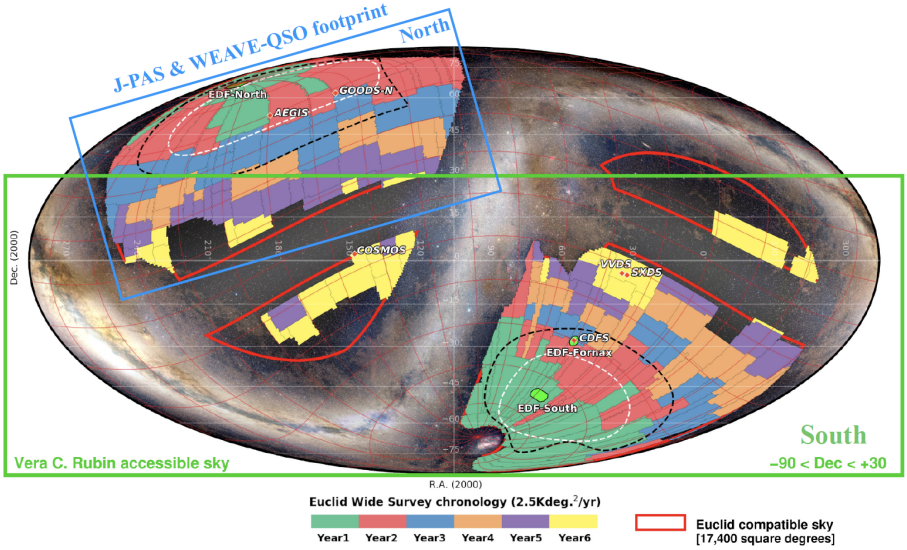

Figure 2: Representation of the full-sky that will be covered the J-PAS, WEAVE-QSO and Euclid survey

In the upcoming years there will be new large-scale surveys providing a high quantity of data of all the sky, being applicable to study cosmic voids resulting in a improvement of the statistics. Offering a unique opportunity to first measure the response of various cosmological observables to the presence of voids, and then to confront those measurements with theoretical predictions. Such mappings will allow us to extract catalogs of voids with denser tracer samples and at earlier (and more distant) epochs. One of the most expected photometric surveys is LSST (2024), due to its big covering of the sky (18.000 deg^2) and its wide-deep field, provided by the largest camera ever constructed for astronomy [38]. We will also have data provided by spectroscopic surveys such as the Euclid survey. It is suppose to finish in 2026 and it is going to bring more information about cosmological objects between $0.9 < z < 1.8$ in a 15.000 deg^2 area [36, 37]. Some of the forecast studies conclude that the exploitation of the cosmic voids in Euclid will provide competitive constraints on cosmology [[6],[5]].

The surveys commented above fell into two different types of category: measure the redshift using photometry (lower z resolution but more galaxies) or spectrometry (higher precision in z but

less galaxies), but there is a third option that is now being explored. These types of surveys use spectro-photometric data, using imaging and narrow band filters, providing larger amounts of data with slightly less precision on their distance. This is interesting for studying cosmic voids, where the error in distance is not that important. One of them is the PAU survey, that uses an imaging instrument with 40 narrow bands with $100 < \deg^2$ [39]. The other one is the J-PAS survey, which is going to cover 8.000 $\deg^2$ with 56 filters, 54 narrow bands and two more broad bands[43, 44]. With its characteristics and some of the forecast studies, seems that it will produce a higher QSOs density than eBOSS survey at high redshift range, being our main goal to prove that in this study.

1.4 J-PAS survey

The Javalambre Physics of the Accelerating Universe Astrophysical galaxy (J-PAS) survey is going to provide an unprecedented amount of information, starting at the end of 2022 with an approximate duration of 5 years. It will have a notable spectral resolution due to their filter system and it will cover about 8.000$\deg^2$ of the northern sky (see Figure 2), using the JST250 Telescope located at the Observatorio Astrofísico de Javalambre (OAJ) in Teruel. The novel and unique aspect of J-PAS lies on its filter system: 54 narrow band (NB) filters, ranging from 3780 Å to 9100 Å, complemented with two broader filters in the blue and red wings [44]. The NB filters have a FWHM of 145 Åand are spaced by about 100 Å, thus creating a continuous spectral coverage through the entire optical range. The filter system has been particularly designed and optimized to achieve a photometric redshift (photo-z) accuracy sufficient to carry out cosmological experiments using a variety of tracers at different redshift ranges (the expected photo-z error of QSOs is $\sigma_z \sim 0.0002(1+z)$ [60]).

With this approximate idea of the characteristics of the J-PAS survey, we created different mock quasars catalogs to study its constraining power. The utilization of quasars as tracer density to identify the voids is because they are an extremely active galactic nuclei (AGN). Their luminosity can reach values of thousands of times grater than the Milky Way, allowing to find cosmic voids at high redshift. J-PAS survey will provide information about more than 3 million of these objects, up to redshifts of $z \sim 6$.

1.5 Challenges and short work plan

The aim of this study is to forecast the constraining power of J-PAS survey using cosmic voids cross-correlations with various of the secondary CMB anisotropies. For this purpose, we create different QSO density mock catalogs. We use an eBOSS-like quasar density as a baseline, and then we create two more catalogs increasing the quasar density in two steps, to get closer to the QSOs catalogs that will provide J-PAS survey. We want to demonstrate that J-PAS survey will be powerful for studying cosmic voids, and that it will also help to advance our knowledge of the high-redshift Universe.

This work is organized as it follows. Section 2 explains in more detail the data used and how the mock catalogs were created. Section 3 includes the methodology used to finding the voids, the explanation of the stacking methodology and the necessary theory to calculate the S/N. The different results are presented in Section 4, and in Section 5 we discuss the main results of this project.

2 Data set

With an approximation of the characteristics of the J-PAS survey [44] we created different mock quasar catalogs to forecast its constraining power. These catalogs have been generated by populating the halo catalog from the Websky simulations with different QSO density, based on an Halo Occupation Distribution (HOD) methodology. It is employed as baseline what an eBOSS-like density

QSO catalog produces, and then we increase this QSO density to be more accurate with the J-PAS survey. This increase in QSOs density is due to the fact that the J-PAS survey is expected to be deeper than eBOSS. Moreover, to study the secondary CMB signals generated by cosmic voids at low redshift, we used the CMB extragalctic maps from Websky.

2.1 Websky galaxy catalogs and masks

In order to forecast the S/N from cross-correlations of J-PAS voids and the CMB maps, we first create different mock catalogs with different QSOs as tracer densities to find the voids. It is anticipated that the narrow-band filter system of the J-PAS survey would accurately identify and measure the redshifts of more than 3 million of these objects, up to $z \approx 6$. This technique is perfect for detecting the broad emission lines of type-1 quasars. This quasar survey will be by far the largest ever conducted, outperforming SDSS by a factor of > 20 and allowing, for the first time, measurement of large-scale structure using only quasars. The search for strongly lensed systems is another exciting application of the quasar survey: J-PAS will provide hundreds of candidates with multiple images. Although this survey has not started yet, it is presented in 2020 the miniJPAS survey data set [44], highlighting key aspects and applications of the spectro-photometric data (see Figure 3). These data have allow to establish the photometric depth and redshift accuracy that J-PAS can achieve.

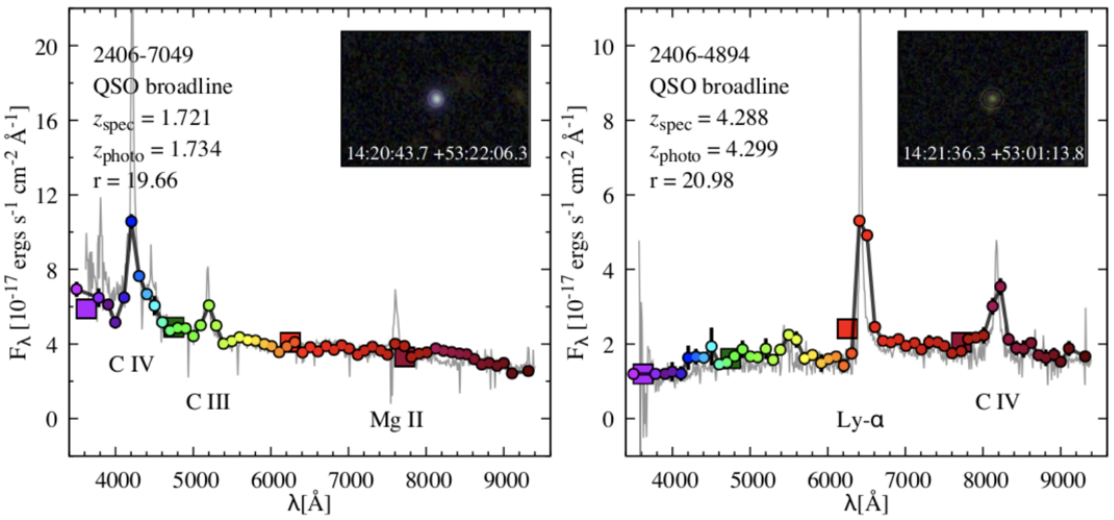

Figure 3: J-spectra of quasars at different photometric redshift,z_{phot} = 1.734 and z_{phot} = 4.299, in the miniJPAS field (colored symbols) compared with the SDSS spectra (gray lines) by [44]

Following this information, we created three different mock QSOs catalogs (task led by Nestor Arsenov, collaborating PhD student at the IAC) using the publicly-available Websky simulations. This public data presents a halo catalog considering all halos within a maximum redshift of $z = 4.6$ and a total survey volume of approximately 1900 Gpc^3. While Websky is not an N-body simulation but based on the approximate peak Patch technique [35], its precision is sufficient for the purposes of this study, considering the relatively large scales of the voids compared to e.g. galaxy clusters where further precision might be needed. The Websky catalog contains 9×10^8 halos, each with an inital Lagrangian position and a final Eulerian position in Mpc, velocity [km/s] and mass [$M_{200\rho_m}$].

At the beginning of this research we started using a general low redshift halo catalog from Websky

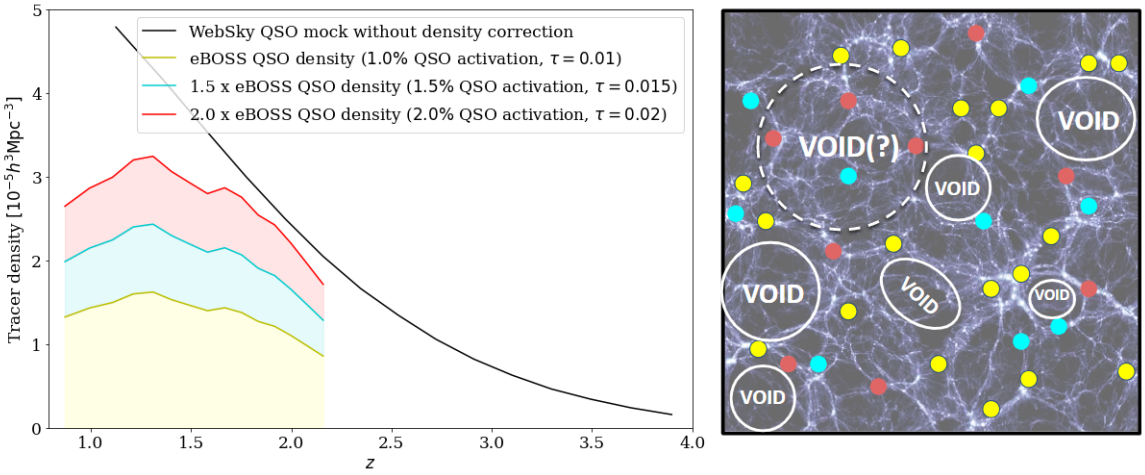

Figure 4: *Left*; Figure produced by Nestor Arsenov (PhD student at the IAC) that shows the tracer density with the redshift. It is represented the different mock catalogs using as a baseline an eBOSS-like quasar density (*yellow line*), and then increase $1.5x$ (*blue line*) and $2x$ (*red line*) the number density of quasars to get closer to the expected J-PAS QSO catalog. *Right*: Portion of the large scale structure of the Universe with an individual representation of the number density of the quasars of each mock catalog. eBOSS-like density mock catalog (*yellow dots*), JPAS low +50% (*yellow + blue dots*) and J-PAS high +100% (*all dots*).

with $z < 0.5$. We test the void finder [32] and then represent the stacking of the diferent CMB maps from Websky. As we are going to see at Section 4.1 we conclude that the best CMB map to use in this investigation is the lensing map. This is because using the CMB gravitational lensing the κ profile of the stacked voids present a higher signal and less fluctuations.

In this project we want to constrain the power of the J-PAS survey populating with quasars the Websky halo catalog between $0.8 < z < 2.2$. This redshift range is the one studied by the eBOSS survey and we want to compare the S/N in a volume equivalent to that but having more QSOs. Starting from the public Websky halo catalogue, the three different mock QSOs catalogs have been produced by using the *github* code called Pyhod. This code allow to populate the dark matter halos with QSOs, following an halo occupation distribution (HOD) approach. There are three mocks created by using three different densities (or quasar distribution over the redshift range, $N_{QSO}(z)$). One mock was created with an analogous density to what has been measured with eBOSS survey. Then, we generated two more mock catalog, the low density QSO $1.5x$ times of the eBOSS mock and the high density QSO with a density of $2x$ eBOSS 4. The $1.5x$ (*J-PAS low*) and $2x$ (*J-PAS high*) density values were chose to approximately model the increment in quasar from J-PAS survey compared to eBOSS survey.

Apart from the galaxy catalog, we need to apply a mask for the mock catalogs and the CMB maps. We created a simple octant mask to model the approximate survey coverage of J-PAS after a few year of observations. This octant mask has a coverage $\sim 5000\text{deg}^2$ being smaller than the nominal $\sim 8000\text{deg}^2$ area that J-PAS will cover. We have used this strategy to safely study the future observations of J-PAS survey, even if the planned full survey area will not be covered eventually. Moreover, since errors scale roughly with $\sqrt{\text{sky area}}$, we can just re-scale the $\sim 5000\text{deg}^2$ errors to $\sim 8000\text{deg}^2$ to update the expected S/N for the actual area measured by J-PAS.

2.2 Websky CMB map simulations

In this project, we chose to study cosmic voids cross-correlating them with the Websky CMB extragalactic maps: the Integrated Sachs-Wolfe (ISW) map, the thermal and kinetic Sunyaev-Zeldovich (tSZ and kSZ) map and the gravitational lensing map (κ) map. Each of them allows us to investigate different degeneracies of the cosmic voids. Each type of effect will be discussed in this Section and in Section 4.1 we explain that the voids cross-correlations will only be studied with the CMB lensing map in this project, because the κ profile presents the highest signal and lowest fluctuations.

The Websky CMB simulations models the evolution of the matter distribution using the mass-Peak Patch method in a volume of $\sim 600(\mathrm{Gpc/h})^3$ with $\sim 10^{12}$ particles over the redshift interval $0 < z < 4.6$ [52]. Despite being an approximate simulated method, mass-Peak Patch has been shown to reproduce the clustering properties of halos with good accuracy for both 2-point and 3-point statistics and their covariances across. The simulation only includes dark matter particles, therefore the baryonic effects are neglected in the analytical modelling, discussed as well in the previous section. This realization of the matter distribution is used to produce full-sky maps of the secondary CMB anisotropy maps: ISW, SZ and lensing. Above all, the ISW effect is sensitive to the dark energy, whereas the gravitational lensing is sensitive to the dark matter, and the SZ effect depends on the baryonic physics. The study of these effects combined is useful to study the Universe. The following sections explain the effects caused by each of the CMB maps and how the different maps have been built.

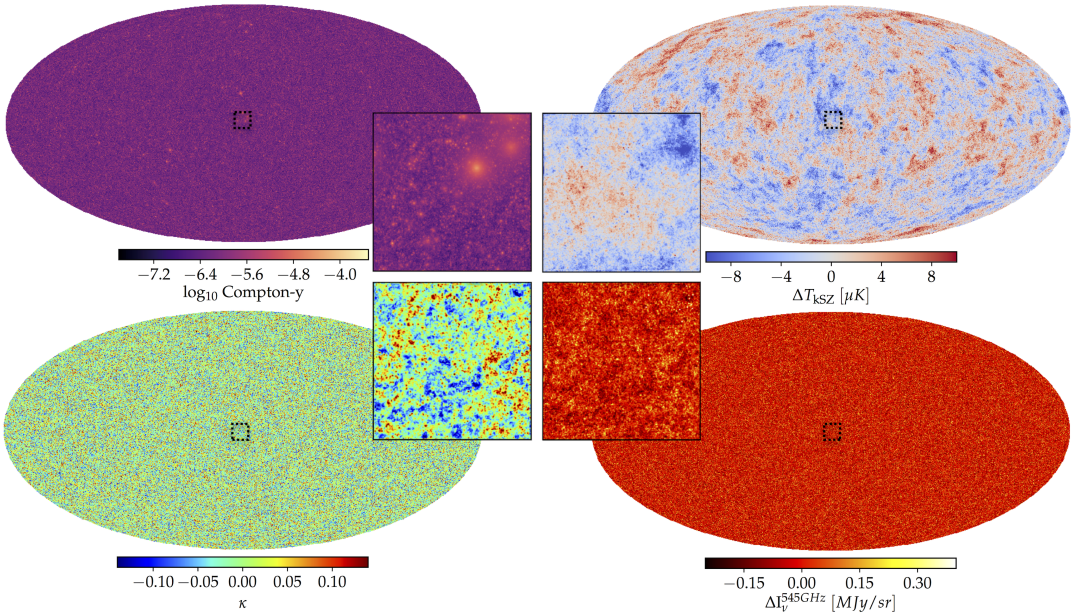

Figure 5: Clockwise from top-left: Thermal Sunyaev-Zel'dovich, kinetic Sunyaev-Zel'dovich, Cosmic Infrared Background, and CMB lensing convergence signals from Websky CMB extragalactic simulations. The central panels show a $10^\circ \times 10\circ$ of each map [52]

2.2.1 Thermal and Kinetic Sunyaev-Zeldovich (tSZ and kSZ) Effects

The Sunyaev-Zeldovich effect (SZ effect) is the inverse Compton scattering [1] of the CMB photons off electrons in any cosmic structure, which cause a distortion in the radiation spectrum of the CMB [50] and produce the most noticeable source of the secondary anisotropies in the cosmic microwave background in sub-degree angular scales. This effect has no dependence with redshift, providing a unique probe of the structure of the Universe at large scales. Additionally, SZ effect is a frequency-dependent source, allowing to be disentangled, e.g. primarily CMB signal, which is ν-dependent, and radio galaxies. Especially, the SZ effect data provides a direct measure of the electrons pressure of the cosmic web, complementary to X-ray observations, and therefore it probes the pressure of the gas in voids or galaxy clusters ([47], [49]). A detailed understanding of the general properties and distribution of gas in different environments is essential for an accurate understanding of the physics of the structure formation. We cross-correlate our data into the two different types of this effect, depending on how cause the interaction: thermal SZ (tSZ) and kinemtic SZ (kSZ) effect.

If the distortion of the CMB is produced due to the energy of the electrons, this is the case of thermal SZ effect. This effect is sensitive to the baryonic matter and it is determined by the Compton y-parameter [31], which is proportional to the optical depth-weighted ratio of electron thermal and rest-mass energies in a given direction, and can be defined as

$$y = \int d\tau \frac{k_B T_e(n)}{m_e c^2} = \frac{8 - 5Y_p}{2(2 - Y_p)} \frac{k_B \sigma_T}{m_e c^2} \int d(1+z)^{-1} P_{th}(n)$$

where P_{th} is the thermal pressure of the gas, $Y_p \approx 0.24$ is the abundance of helium, and the medium is assumed to consist of fully ionized hydrogen and helium. This expression is only valid if $T_e >> T_\gamma$. The cross-correlations with tSZ of cosmic voids, probe the presence of hot gas in low density regions as well as some of its properties (study of the gas temperature-density relation)[30].

With this description of the effect, the CMB tSZ maps (see Figure 5) were created by projecting the pressure profiles determined from the hydrodynamical simulations of [55] onto the mass-Peak Patch halo catalogue to create the Websky Compton-y map, using all $\approx 9 \cdot 10^8$ halos and it did not consider the contribution from the field [52].

On the other hand, the kinematic Sunyaev-Zeldovich effect is due to the scattering of moving electrons in the Universe with respect to the rest frame of the CMB. The kSZ is a physical process of electron-photon scattering which keeps the CMB spectrum almost unchanged, while the thermal Sunyaev-Zeldovich (tSZ) is a process that changes the CMB spectrum.

We define this effect through the temperature as [31]

$$\frac{\bigtriangledown T^{kSZ}}{T^{CMB}} = -\int d\tau v(\chi\hat{n})\hat{n} \tag{1}$$

where χ is the comoving distance, n_e is the number density of the comoving electrons and τ is the Thomson scattering optical depth.

The kinetic Sunyaev-Zel'dovich map (see Figure 5) contains both a spherical halo profile, and a clustered field component ($\bigtriangledown T^{kSZ}_{halo}(\hat{n}) + T^{kSZ}_{field}(\hat{n})$) containing the electrons in the intergalactic medium and unresolved halos. These include different contributions from different investigations ([56],[57]), apart from the halos and the field (To more detail see [52]).

[1] Scattering of low energy photons (CMB) to high energy electrons (cosmic structures)

2.2.2 Integrated Sachs-Wolfe (ISW) Effect

At a certain time ($z < 1.5$) when the Universe was undergoing a transition to a dark energy dominating phase, was when the expansion started to accelerate. The large-scale gravitational potential (galaxy clusters and cosmic voids) energy evolves with time because of that acceleration, producing a subtly changing of the gravitational potential of photons passing through them.

When a photon enters in a supercluster, it gains the proportional potential well, but when this photon leaves this structure, it does not lose of all of the energy it gained, because in the meantime the potential got slightly shallower due to dark energy, and this means a slightly hotter temperature. In contrast, when a photon crosses a cosmic void, the change of the gravitational potential cools the photons, reducing their energy. This effect is called the Integrated Sachs-Wolfe.

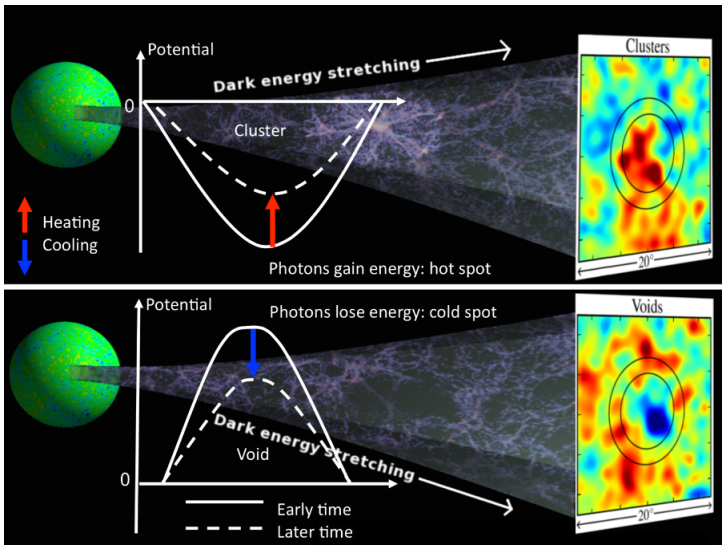

Figure 6: Representation of the ISW effect in clusters and voids, caused by the accelerated expansion of the Universe. This causes a subtle change in the photon energy passing through them. *Top:* When a photon enters in a supercluster, it gains the proportional energy of the potential well, and after that photons give back less when they exit the potential, which in the meantime has got shallower (**Hot spot**). *Bottom:* When a photon passes through a cosmic void, the change in gravitational potential cools the photons, reducing their energy (**Cold Spot**).

The ISW effect is the dominant effect in the late-time evolving Universe of the secondary anisotropies, whereas exist another contribution minus dominant and non-linear, named Rees-Sciama effect ([54]). We focus on the linear ISW effect, having a good theoretical definition of its temperature along the direction, n̂

$$\frac{\triangle T^{ISW}}{\overline{T}}(\hat{n}) = -2\int_0^{z_{LS}} a[1 - f(z)]\Phi(\hat{n}, z)dz \tag{2}$$

where Φ is the gravitational potential, $f = \frac{dlnD}{dlna}$ is the linear growth rate of structure and a the scale factor. These ISW imprints on the temperature fluctuation of the CMB can be measured in cross-correlation with the matter distribution such as cosmic voids. Assuming a flat universe, then a detection of the ISW represents a measurement of the dark energy and its properties [41].

2.2.3 Gravitational lensing Effect

The presence of the large scale structures of the Universe produce a deflection of photons along the line of sight, called gravitational lensing. This was predicted by Albert Einstein in the general theory of relativity [1]. This effect is the deviation of light trajectory due to gravity, caused by the curvature of the space-time due to a massive object.

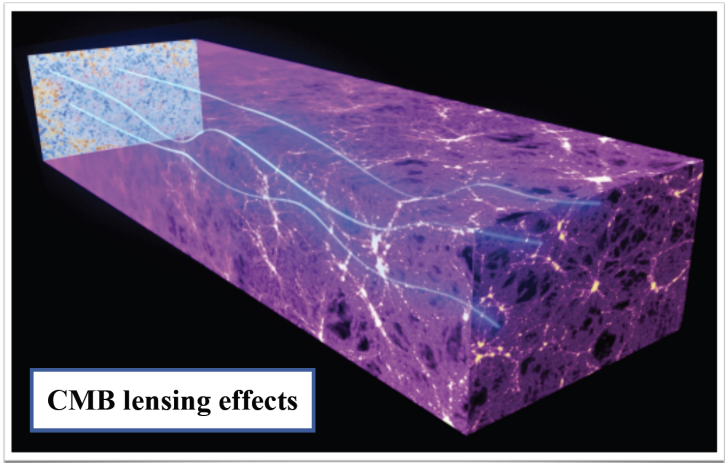

Figure 7: This illustration shows how photons in the Cosmic Microwave Background (CMB) are deflected by the gravitational lensing effect of massive cosmic structures as they travel across the Universe.

There are different types of gravitational lensing: strong lensing, weak lensing and microlensing. Strong gravitational lenses are cases where a distant object (galaxy or quasar) is align so closely with a foreground galaxy or cluster of galaxies that the gravitational field of the foreground object creates multiple, highly distorted images of the background object [33]. When the lens is not strong enough to form multiple images, but still the source is distorted, this is called the weak gravitational lensing [51]. This type needs a statistical study of the deformation of the cosmic structures, performing an analysis of the distorted shapes (shear and magnified) of background galaxies in a given direction, assuming that galaxies are randomly orientated. Measuring this effect gives us information about the foreground matter distribution, including dark matter.

With the CMB data we do not have information about distortions of galaxy shapes, but a lensing convergence map can be reconstructed from the non-gaussianities of the CMB temperature patterns. Therefore, the magnification due to the weak gravitational lensing can be defined by the convergence, described by κ. This parameter define the isotropic distortion of a source, contraction or dilation, and is express as

$$\kappa(\theta) = \frac{3H_0^2\Omega_m}{2c^2}\int_0^{r_{max}} \delta(r,\theta)\frac{r(r_{max}-r)}{r_{max}}dr \tag{3}$$

Where H_0 is the Hubble parameter, Ω_m is the matter density parameter, δ is the matter density field and r_max is the maximum co-moving distance to source galaxies considered. Moreover, the κ parameter can be computed from the gravitational potential as $\kappa = \frac{1}{2}\bigtriangledown^2\,\phi$.

The Websky CMB convergence map of the primary CMB is constructed using the field particles and an NFW (Navarro, Frenk, White) profile for all halos in the mass-Peak Patch halo catalogue that subtend more than a pixel, since lower mass halos are not resolved [52]. In this study, as we

explain in section 4.1, the cross-correlation with the cosmic voids will be study only with the CMB lensing map.

3 Methodology

In order to forecast the constraining power of the J-PAS survey with cosmic voids, we use different mock catalogs that reproduce the QSO density of J-PAS and eBOSS. Then, we ran a 2D void finder to cross-correlate the cosmic voids with the Websky CMB maps using and stacking methodology. We also calculate the S/N of the κ signal of cosmic voids to calculate the power of J-PAS survey.

3.1 2D void finder

To find cosmic voids there are different existing algorithms, like Voronoi Tesellation and growth of spherical structures. In the literature most of the algorithms used data of spectroscopic redshift surveys (BOSS), but they require a long observation time and are restricted in depth. Alternatively, data from photometric surveys (DES) are more efficient and deeper, but the redshift information is less accurate. In our study we use the 2D void finder algorithm created by [32] which was developed to deal with photo-z data sets. The 2D void definition has illustrated a high potential for extracting void lensing signals in simulations, demonstrating robust detections from observed and simulated data [23]. Despite the fact that numerous studies using 3D voids algorithms have demonstrated that they can successfully detect void lensing signals, a full 3D information using photo-z data set is inaccessible due to smearing effects in the line-of-sight.

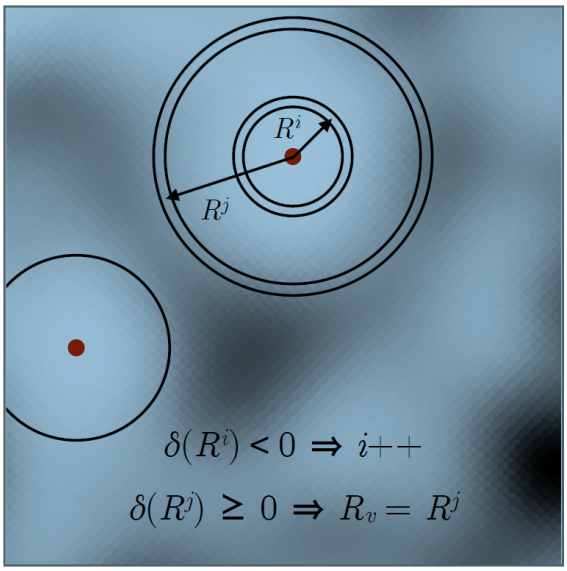

Figure 8: Description of the 2D void finder algorithm [32]. The background field is the smoothed galaxy field ($\sigma = 10$ Mpc/h) and the two red points show two void centers. The R_i, represents the starting radius of a circular shell. When the density contrast reaches $\delta(R_v^j \geq 0)$, the void radius is defined as $R_v = R_v^j$.

The 2D void finder method works by projecting galaxies in 2D redshift slices and finding voids in the defined minima of the smoothed quasar field in the given slice, allowing to detect a void

that is not completely empty of galaxies. The algorithm select the galaxies in a given redshift slice, we use a thicknes of 100 Mpc/h, and then project them into a HEALPix map with a resolution of $N_{side} = 512$. With the projected galaxy map and the corresponding smoothed contrast map, defines voids as underdense circles in the projection, with their center located in a local minima of the smoothed field. It starts defining circular shells of increasing radius (R_v) around the center, and stops when then mean density within the slice ($\delta = 0$) in its outer shell of the void is reached. The R_v is measured in degrees, but the algortihm converted to units of Mpc/h assuming the best-fit Planck Cosmology 2018 [12].

The void catalog produced by the algorithm depends on three main free parameters. One aspect of this project is devoted to determining the best-fit parameters for the J-PAS data, which yields the highest κ signal and the greatest number of *genuine* cosmic voids. Because searching the maximum voids may result in finding many *spurious* voids (empty spaces that the 2D void finder recognize as a void) which derives an increase of noise in the data.

- *Smoothing scale* in co-moving distance, σ. Chosen in [32] as $\sigma = 10$ Mpc/h, to be half the radius of the smallest voids in the data sample. This parameters defines the Gaussian smoothing scale that we apply on the density map to define the minimum of the density. With a higher σ the algorithm is going to find less voids, because it is going to produce a merger effect of smaller voids into larger voids. Therefore, this parameter change the number of voids and also, the mean R_v.

- *Underdensity threshold*, δ_{min}. In a smoothed density map this parameter defines the minimum density number of a void and the number of underdensities that chose as a unique or more void. Working with a lower threshold will imply a higher number of voids.

- *The slices thickness*, s. It was determined that a thickness of $100h^{-1}Mpc$ leads to the detection of independent and individually significant underdensities [32].

Apart from the three free parameters, there are the definition of the input galaxy data in the algorithm: Ra, Dec and redshift. Moreover, we enter the redshift range to study. In this project, mostly we use $0.8 < z < 2.2$. Thechnically, the code work in $h^{-1}Mpc$ units, not z, and we convert them using the standard ΛCDM cosmology with $h = 0.68$ and $\Omega_{m_0} = 0.3$.

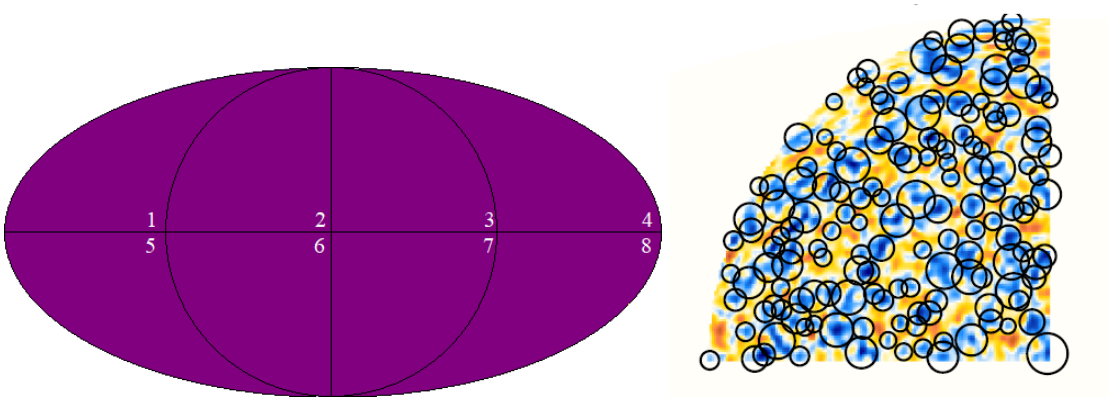

Figure 9: *Left*: Depiction of full-sky map divided by each of the 8 octants. *Right*: Representation of the second octant of the sky illustrating the cosmic voids founded with the 2D void finder algorithm.

The aforementioned process gives the information of each void in a given redshift slice. Apart from the position, redshift and radius of the cosmic voids, it generates two additional parameters that are used to filter the data in this project. Taking into account the δ, when the void reaches the mean density in its outer shell ($r < R_v$) and δ_c, when the inner part of the void ($r < R_v/4$) surpasses the condition $\delta = -0.8$. Another point to consider is that the code allows to run the full-sky, but we mask the data using one octant (figure 9). The reason is that J-PAS will not cover all the sky area and we are interested in seeing how big are the fluctuations between octants, that could be relevant when interpreting J-PAS results in the future. We anticipate that a homogeneous and isotropic Universe should presents small differences between octants, but we still wanted to check it with our data (see Section 4.2).

3.2 Stacking methodology

Studying the cosmic voids in simulations or through observation data individually is difficult because normally the signal is not high enough [20] and the cosmologically interesting signals associated with these regions are noisy. The current best solution is to use the stacking methodology, an established technique in the field. This method, applied to cosmology [45], needs a high number of voids to make good statistics, but as a result there is a decrease of the noise in the data. Moreover, the shape of individual voids can be complex, but considering an isotropic and homogeneous Universe, the average shape of voids is spherical, allowing to apply the Alcock-Paczynski test [46], with reduced systematics.

We applied the stacking methodology to measure the imprints of the voids lensing signal. This method cut-out squared shapes patches from the CMB map aligned with the center position of each void, using the HEALPix package. Then we do a relative re-scaling of all the size of the cut-out image knowing the radius of each void (R_v). Finally, we measure the mean signal of all the stacked patches. The best parameters to use in the stacking process [32], is a cut-out size of the box of 200 pixels, define as xsize, of the CMB and a 10 R/R_v number of voids radius in this xsize. Apart from studying cosmic voids with the stacking image, we can measured the tangential signal profiles from the stacked images using a 25 bin resultion.

One other thing to consider, is to filter our data produced in the void finder algorithm, before the stacking takes place. We use a $R_v > 20$ Mpc/h, $\delta_{min} < -0.3$ and $\delta < -0.05$, taking the criteria from the literature [32].

For all the voids catalogs cross-correlated with the CMB maps, we apply some sort of pre-processing, to adapt it to our data. The Websky CMB maps are provided with a pixel resolution of $N_{side} = 4096$, but given the nature of this project we downgraded the high resolution map to a lower $N_{side} = 512$ and we change to the typical units specifically for each signal. Secondly, we have applied a small Guassian smoothing with $FWHM = 1^\circ$ to suppress noise contributions from small-scale fluctuations, and also we make a removal of the large scale modes ($\ell < 10$ cut), this is a frequent correction in the literature that aids in data cleaning. To check its effect, we measured the κ signal with and without these large $\ell < 10$ modes and the smoothing (see Figure 10). We found no significant difference with or without the $\ell < 10$ cut, so we decided to use it to reduce systematic effects. Thirdly, we remove the bias from the CMB map and the mask. This bias is the mean of the Websky κ map in a given octant, and we remove it to deal with a zero-mean fields in the stacking, where the expectation is that far away from voids the signal will converge to zero. As a last step, we applied the octant masks to the data.

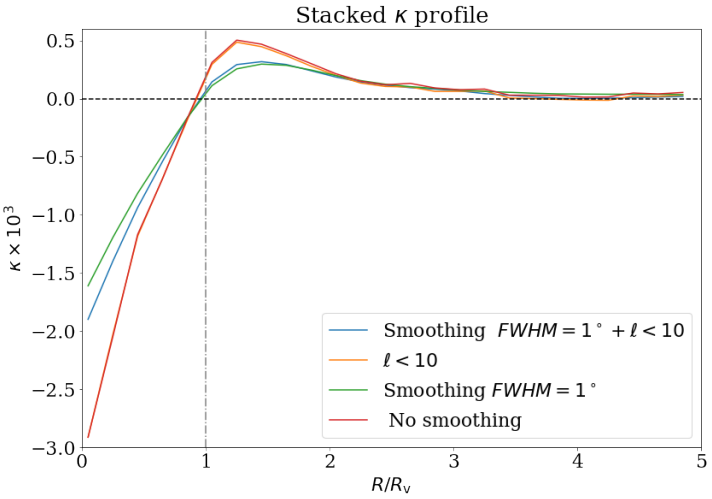

Figure 10: Comparison of the stacked κ signal profiles, of the cosmic voids in J-PAS high mock catalog using $\sigma = 30$ Mpc/h and $\delta_{min} = -0.2$, applying different smoothing of the CMB κ map: the Gaussian smoothing with $FWHM = 1^{\circ}$ and the removal of the large scales modes. The first suppress the noise contribution of the small scales and the second removes the large scale structures ($\ell < 10$). In our data we applied the smoothing (FWHM $=1^{\circ}$) + $\ell < 10$ cut, because even the signals also drop when we applied both of them the noise also gets smaller and we gain in S/N.

3.3 Random simulations

To account for the simulated data of uncertainty in the cross-correlations, we created 1000 random realizations of the fluctuation signal of the CMB κ map and also random noise maps using the power spectrum released by Planck team [48]. The second one is the dominant source of uncertainties in the stacking measurement. Moreover, we have to consider the contribution of the fluctuations of the signal map itself. This second contribution is because when we build the stacking κ signal of the voids, they are not totally isolate, there are possible overlaps along the line-of-sight, which implies a reconstruction with imperfections.

Following [23], we measure the power spectrum of the fluctuations in the Websky κ map with the HEALPix anafast routine. Then, with the synfast routine of HEALPix, we generated the 1000 random realizations of the Planck-like noise map (N_k^i), knowing its power spectrum. Adding the simulated CMB lensing signal map to the randomnly generated noise maps, to model the noise, we generate 1000 more random realizations of the κ map using the same routine (S_k^i). The signal noise map has no true correlations with the voids, as it takes the statistics of the power spectrum measured to create each S_k^i randomly. After combining the random noises, $N_k^i + S_k^i$. Finally, all the 1000 random realization are stacked on the positions of the voids to later characterize the standard deviation of the fluctuations in such cross-correlation measurements, to be able to produce the error bar of each bin in the stacked κ profile (see Figure 11).

The data used in the creation of the random realization only ocuppy one octant in the sky. This area is consistent with expected sky area of the J-PAS survey from a few years of observations.

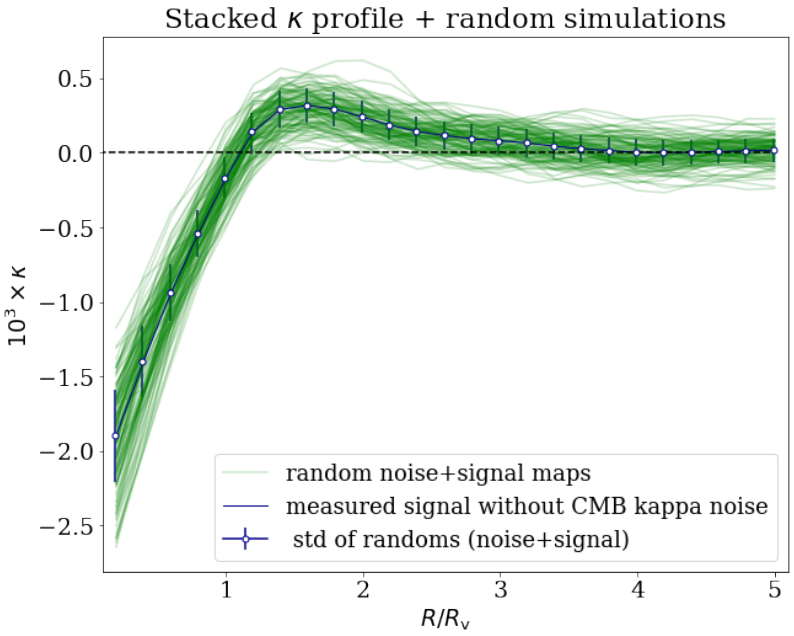

Figure 11: Stacked κ mean profile of the cosmic voids with the error bars. We use the 1000 random realizations (*Green lines*) of the random noise from Planck Team [48] + κ signal to calculate the error bars and the covariance matrix.

3.3.1 Signal to noise

We calculated what an eBOSS-like survey could show in terms of CMB κ signal-to-noise (S/N). And then, increasing the QSO number density in two steps ($1.5x$ and $2x$) and calculating the errors we will see how much J-PAS can improve on that baseline.

To constrain the S/N, firstly we calculate the covariance and the correlation matrix (normalized covariance matrix) using 1000 random realizations, to estimate a robust covariance matrix. This matrix shows how much the data points are correlated with each other (See Figure 12).

This is an example of the covariance matrix formula of two variables:

$$Cov(X,Y) = C_{ij} = \sum_{i=1}^{n}(x_i - \bar{x})(y_i - \bar{y})$$

We then invert the covariance matrix C^{-1}, to calculate the χ^2 statistic:

$$\chi^2 = \sum_{ij}(\kappa_i - A_k\kappa_i) \cdot C_{ij}^{-1} \cdot (\kappa_j - A_k\kappa_j)$$

where κ_i is the mean lensing signal in a radius bin and A_k is the amplitude parameter. In [23] and [58] the objective is to constrain the best-fitting A_k parameter between real data and simulated data, but in this project we only work with the simulated data. Because of that, it is known that the maximum of the likelihood is going to be at $A_k = 1$. We can equally evaluate our data and calculate the S/N defining the amplitude as an interval $-1 < A_k < 3$, with a separation of 0.001 to calculate the χ^2.

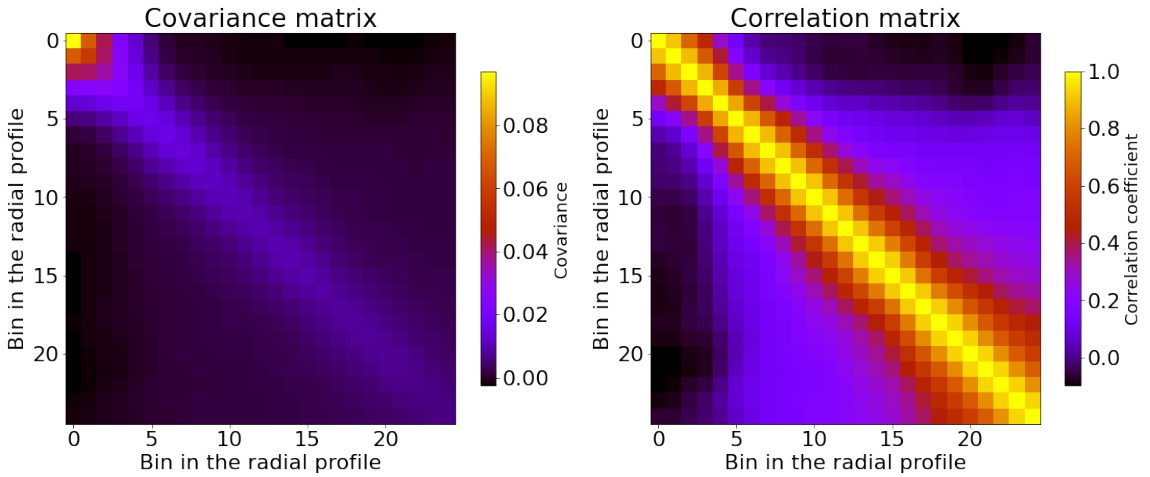

Figure 12: Image representation of covariance matrix (left) and the correlation matrix (right), needed to calculate the χ^2. The off-diagonal contribution due to bin-to-bin correlations affects the S/N estimation.

We determine the value of χ^2 over the matrix and then convert to a probability, approaching it to a Gaussian distribution $\mathcal{L} \sim e^{-\chi^2/2}$. If it shows a narrower function (see Figure 13) we are going to have a better constraining power in our data. Then, with the maximization of the likelihood normalized we can calculate the S/N of the CMB signal of the cosmic voids identified the 68% of the confidence regions about the mean value.

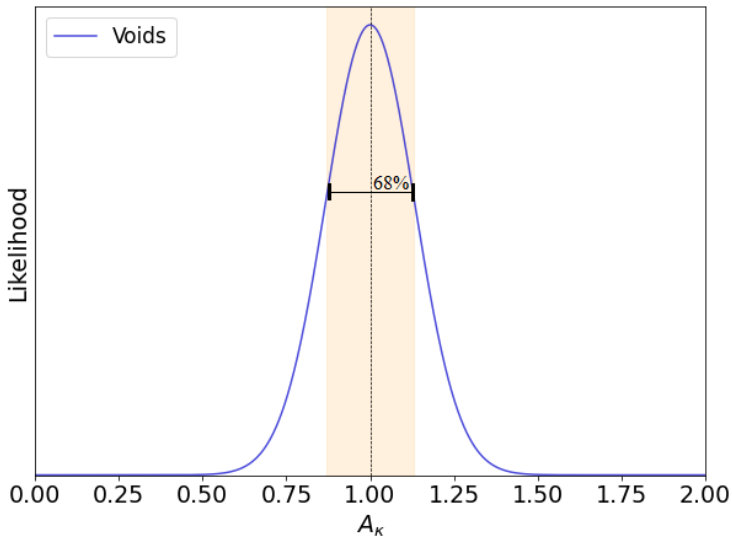

Figure 13: Representation of the likelihood, used to calculate the S/N of the κ signal with the 68%

This overall error estimation and likelihood only works if the errors are Gaussian which is a good approximation in similar measurements presented in the literature [23].

4 Results

In this Section we will go through all the results obtained in this work. We present each CMB signal (ISW, SZ and lensing) from cosmic voids using the low-z catalog and CMB maps from Websky simulations. Then, working only with the CMB lensing map, we generated the κ profile of the cosmic voids using different underdensity thresholds and smoothing scale parameters, to see which combination is the optimal. With $\sigma = 30$ Mpc/h and $\delta_{min} = -0.2$, we studied in more detail the differences between each mock catalog. Finally, we have delved deeper into the J-PAS high-density mock catalog, considering the photo-z error in QSOs and extending the redshift range up to $z < 2.8$.

4.1 Websky CMB comparison

We measure the stacked imprint of the different CMB maps cosmic voids using the Websky low-z halo catalog data. The results are represented in Figure 14, showing the mean staked image and profile imprint of ISW, SZ and lensing effects of 8275 cosmic voids at $z < 0.5$. To find the cosmic voids in the halo catalog we use the parameters $\delta_{min} = 20$ and $\sigma = -0.3$ in the 2D finder, following the studies of [58] and [59].

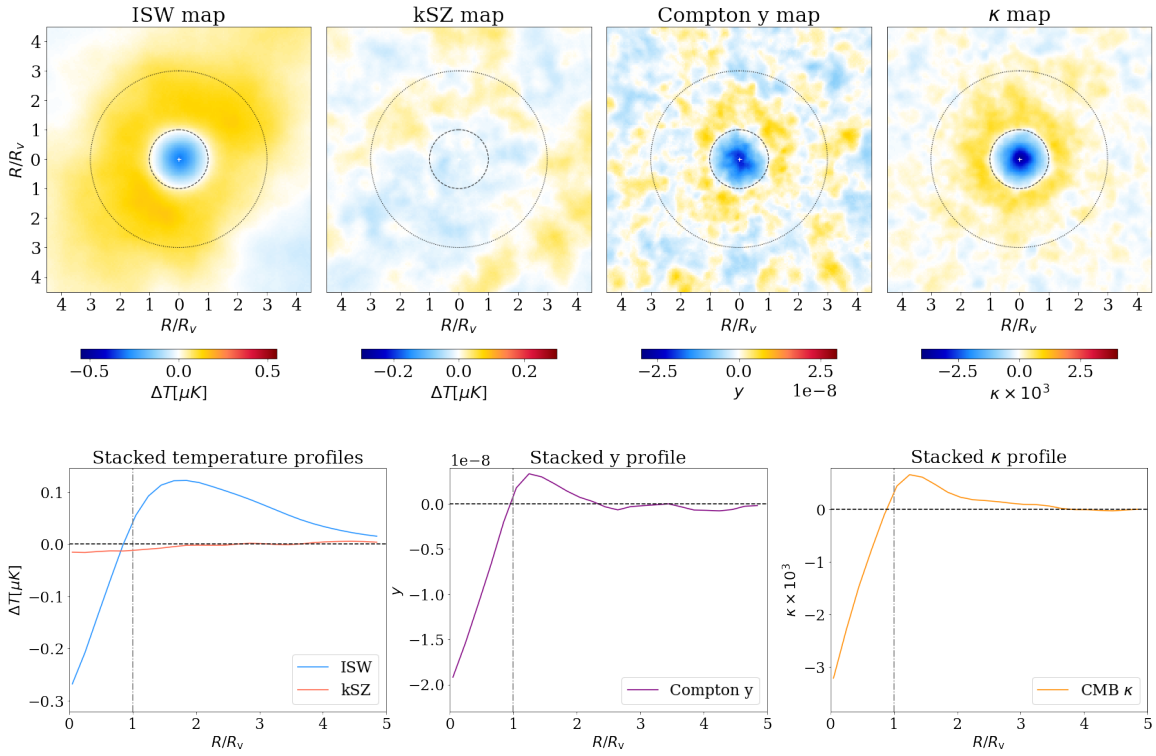

Figure 14: *Top*: Stacked CMB images and *Bottom* profiles from the low-z cosmic voids of the different Websky CMB maps: ISW, kSZ, tSZ and lensing map. At the stacked images, the dashed (dotted) circle marks one (three) void radii in re-scaled units. The observed data displays that the highest signal with less fluctuations comes from the κ CMB map.

The tSZ map presents the highest fluctuations, but with a great signal at the center of the stacked

voids ($y \approx -2$). The lowest fluctuations are at the ISW and lensing stacked CMB maps. In [23] the signal at the center of supervoids in $0.8 < z < 1.2$ of the MXXL simulation is about $\bigtriangledown T_{ISW} \approx -1K$, in our work the minium signal found in the center of the stacked voids is $T_{ISW} \approx -0.6K$ for *general* voids. Taking into account the fluctuations and the highest signal, the best stacked CMB map to use for the Websky simulations is the lensing CMB map.

As we said, we extracted the above cosmic voids from the Websky catalog of halos with $z < 0.5$. In this project, we are going to work with different QSOs density mock catalogs at $0.8 < z < 2.2$. This redshift range in QSOs has only been studied by the eBOSS survey; therefore, the goal of this study is to compare it to the future QSOs J-PAS catalog, which is expected to make deeper observations and produce a higher number of QSOs density. At this redshift range, the 2D void algorithm will find a higher number of cosmic voids. We anticipate improved statistics in the data, which will result in less noise and a higher S/N ratio compared to [58]. Moreover, the CMB lensing kernel (efficiency) is expected to peak at $2 < z < 3$ (see Figure 15), which is close to our data, resulting in a increase of the κ signal. But working at a higher redshift the tracers will be more sparse and the possibility of finding spurious voids is higher.

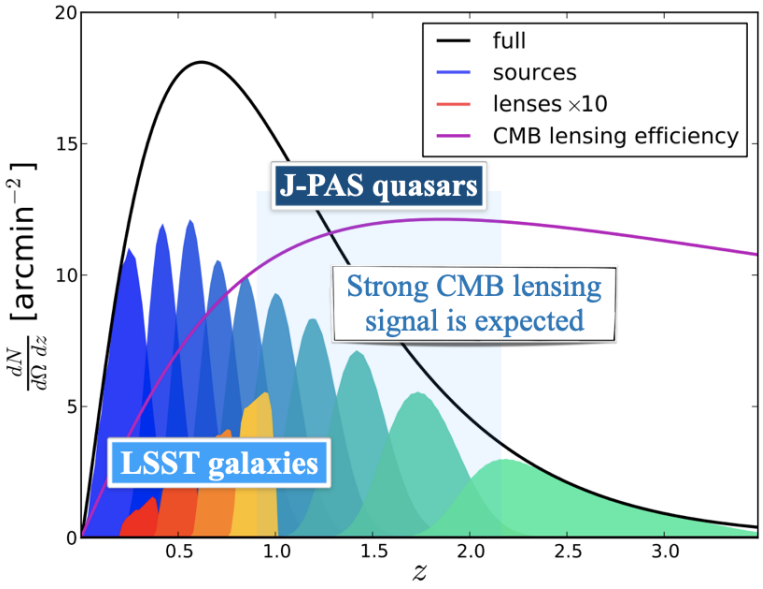

Figure 15: CMB lensing *efficiency* as a function of redshift. At $2 < z < 3$ the CMB lensing signal is expected to be strogner.

4.2 Parameter comparison of Stacked CMB κ maps

To characterize the best expected stacked κ signal of the three QSO density mock catalogs, we generate the κ profile of each one and also calculate the total number of voids using a different parameter setting (σ and δ_{min}). Increasing the value of the σ implies less number of voids, and a lower δ_{min} has the same effect 1, validating the explanation given at Section 3.1. Moreover, we can see that in each combination of data, the mock catalog that presents the highest number of voids is the eBOSS-like density, and the lowest is shown in the J-PAS high-density catalog.

Firstly, we wanted to show that the κ profile of each octant has no statistically significant differences in each mock catalog (see Figure 16), which means that working with the stacked *mean* κ signal has no substantial changes and also reduces the fluctuations of the mean κ profile.

We considered different initial underdensity thresholds and smoothing scales applied to the density field to define the void centres. The total number of voids and mean void size, as well as the resulting lensing signal and noise, are affected by these parameters. In [32], [23] and [58] the minimum smoothing scale normally used is $\sigma = 10$ Mpc/h, chosen to be about half of the smallest radius that we can access in the data sample, whereas in this project we used $\sigma > 30$ Mpc/h. This is because all of these researches studied cosmic voids at $z < 0.9$, whereas we focused our study on voids at higher redshifts, $0.8 < z < 2.2$. At this redshift range the reconstruction of the sky is more sparse, with fewer quasars, which affects the determination of voids and, using a low smoothing scale ($\sigma < 30$Mpc/h), the probability of discovering a large number of spurious voids is high. Then, we varied the underdensity threshold, knowing that the most significant voids found in [32] were employing $\delta_{min} = -0.3$.

Number of cosmic voids in 1 octant

σ[Mpc/h]	δ_{min}	J-PAS high	J-PAS low	eBOSS
50	-0.15	1707	1921	2001
40	-0.1	3449	3741	3975
40	-0.2	2339	2648	2941
40	-0.3	1328	1587	1957
30	-0.2	4754	5076	5728
30	-0.3	3280	3694	4369
20	-0.3	8647	9754	10167

Table 1: Number of the cosmic voids in one octant found by the 2D void finder in each mock catalog with different combinations of the smoothing scale (σ) and the underdensity threshold (δ_{min}).

To know which parameter is the best-fit, we compare the number of voids and, at the same time, the κ profile. We look for the highest number of voids combined with the greatest κ signal (more negative). The highest number of voids are presented in $\sigma = 30$ Mpc/h with $\delta_{min} = -0.2$ and $\sigma = 40$ Mpc/h with $\delta_{min} = -0.1$, respectively, in each mock catalog. In the stacked κ profiles, the highest signal, between this two parameters setting, is presented by $\sigma = 30$ Mpc/h with $\delta_{min} = -0.2$ in the J-PAS high and J-PAS low. And in the eBOSS mock catalog, the greatest κ in the interior of the stacked voids is for $\sigma = 20$ Mpc/h with $\delta_{min} = -0.3$, but most of the voids are spuriuos voids due to the low density of tracers. Therefore, with all these information we conclude that the best-fit parameters are $\sigma = 30$ Mpc/h with $\delta_{min} = -0.2$ for each mock catalog.

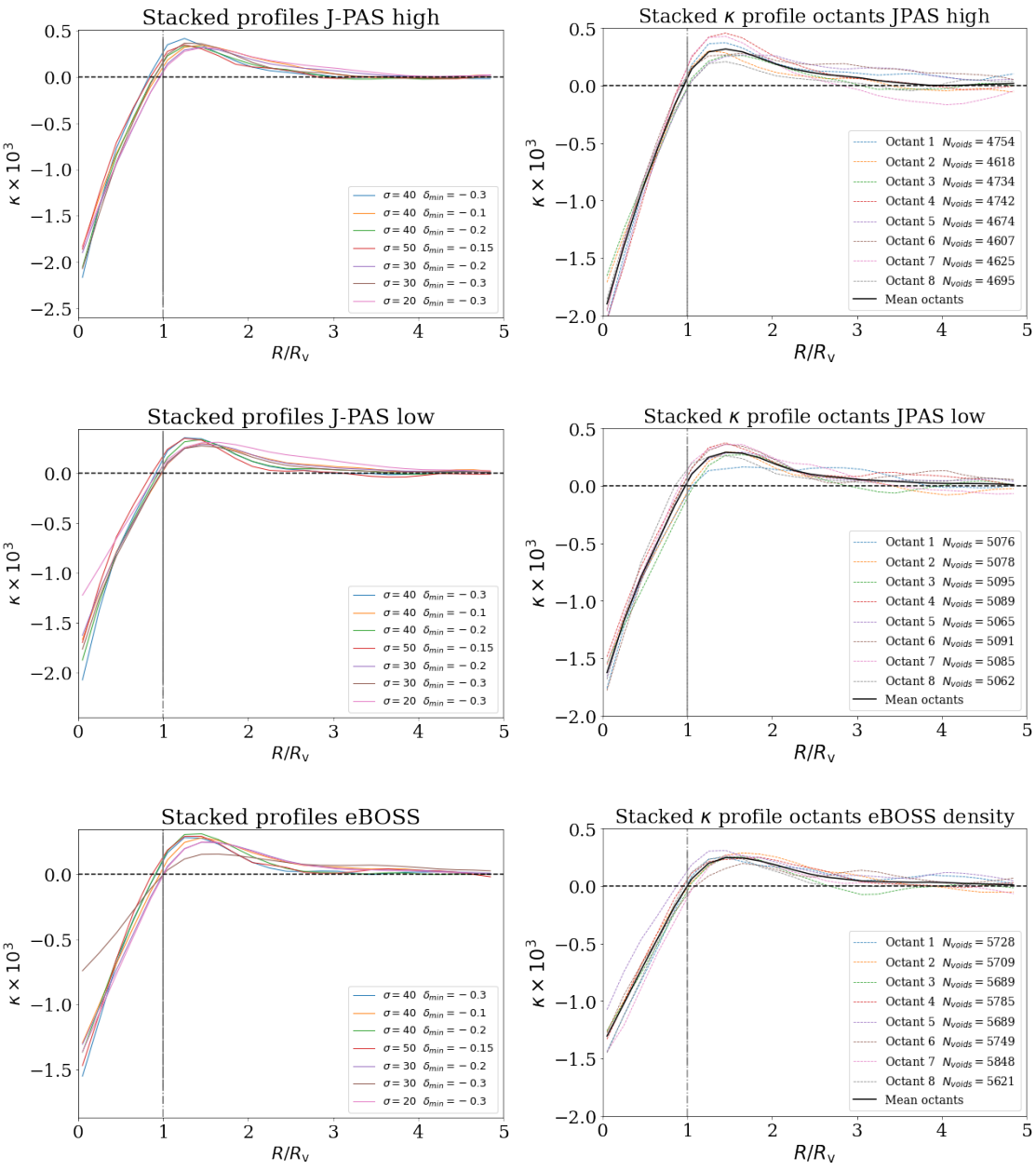

Figure 16: *Left:* Stacked κ profile of cosmic voids using different parameter combinations for each mock catalog. *Right:* Representation of the differences between the CMB κ profile of each octant and the mean of the octants (black lines). It illustrates that the differences between octants are small.

4.3 Mock catalogs with $\sigma = 30$ Mpc/h and $\delta_{min} = -0.2$

With the best-fit parameters defined as $(\sigma, \delta_{min}) = (30\text{Mpc/h}, -0.2)$, we follow the methodology to generate the κ signal of the three different mock catalogs, to estimate the covariance using 1000 random realizations and calculate the Signal to Noise. With this data analysis we aimed to test the hypothesis that the J-PAS lensing voids signal will have a better constraining power than eBOSS survey.

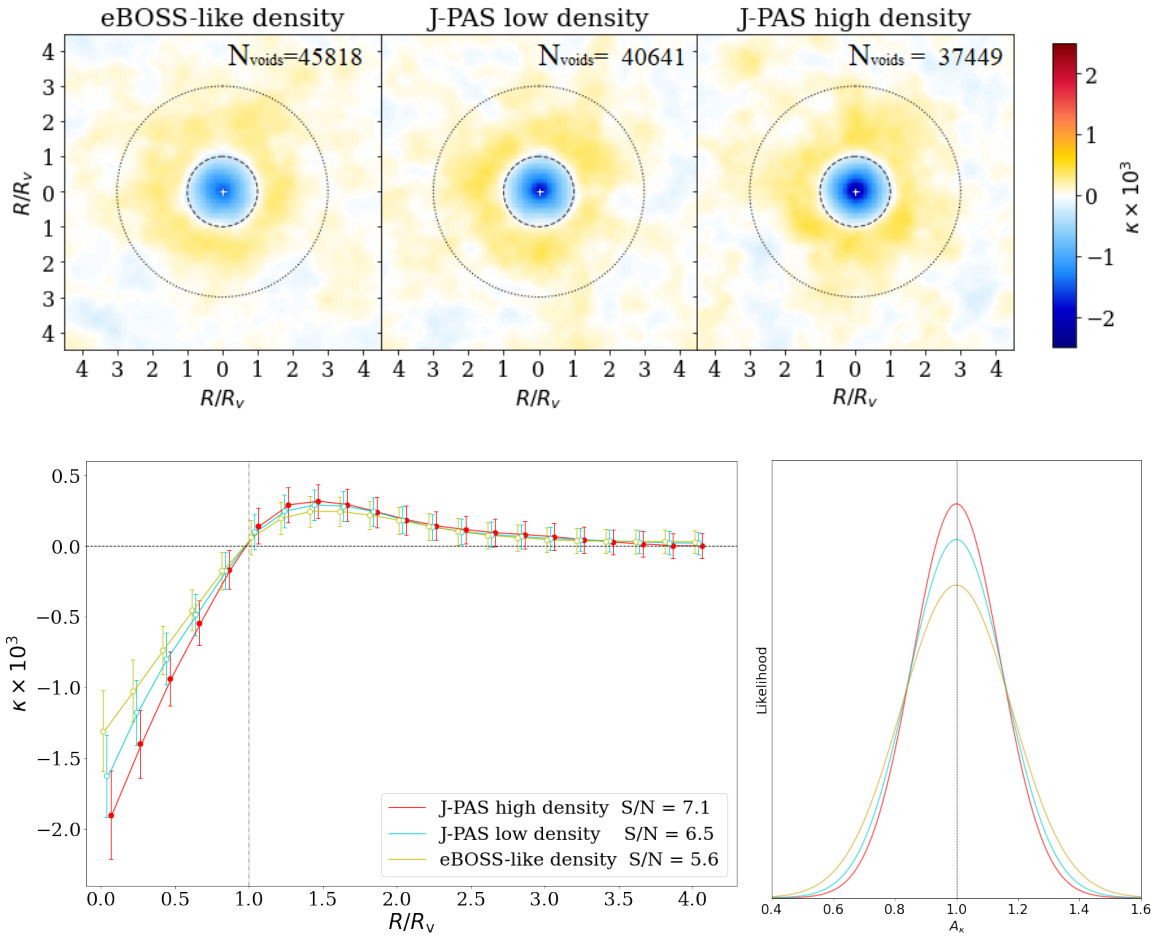

Figure 17: Using the best parameter setting, $\sigma = 30$ Mpc/h and -0.2. **Top**: Stacked CMB κ image from eBOSS-like, J-PAS low and J-PAS high mock catalogs, showing the number of the stacked void in each representation. The J-PAS high mock catalog presents a higher κ signal at the innermost parts of the stacked voids profile, whereas the number of stacked voids found is the lowest. *Bottom-left*: Stacked CMB κ profile with error bars, using 1000 random realizations of the Planck-noise map (N_k^i) + κ map (S_k^i). We detected a strong κ signal (more negative) from the J-PAS high. *Bottom-right*: Representation of the likelihood in each mock catalog, used to calculate the S/N. It shows that a narrower probability presents a higher S/N.

In the κ images and profiles (Figure 17) of each mock catalog we detected a clear negative CMB κ imprint from voids in the central region. We also found a slightly positive κ signal in the surrounding of voids. This compensating over-dense regions is where the matter evacuated from the cosmic voids accumulates and it mark the edges of the voids.

The 2D void finder, with the characteristics described above, identified 37449 and 40641 for the J-PAS high density and J-PAS low density mock catalogs respectively, for the full sky area. To compare with, using the same methodology, we found 45818 number of voids in the eBOSS like-density mock catalog. Although we found more voids in the eBOSS mock catalog, the largest (more negative) κ signal is presented by the J-PAS survey high, since it reaches a higher value of κ in the interior of the void, whereas J-PAS low and eBOSS-like catalogs show a lower value (see Figure 17). The reason for the higher signal is because we can reconstruct the position of the void centers much better, given the higher QSOs density, and this helps to detect a deeper κ imprint. Moreover, and also related to the lower density of QSOs, there is a problem with the spurious voids in eBOSS, which decrease the detectable signal since they do not add a real contribution, just random κ map positions.

To perform the stacking methodology we use the full-sky map, but the J-PAS survey will only cover approximately only one octant, as well as the existing data from the eBOSS survey. Therefore, to get closer to the real data, we generate 1000 simulations by applying a simple octant mask to the lensing map, using the methodology explained in Section 11. The random realizations allow us to produce the error bars of the κ profile and also generate the likelihood normalization. Given these measurements, we aim to constrain the S/N of each mock catalog.

The highest S/N is achieved by stacking 4754 voids of one octant of J-PAS high mock catalog, presenting the narrower likelihood. We estimated a value of $S/N = 7.1$, whereas in J-PAS low ($N_{voids} = 5076$) the value is lower, $S/N = 6.5$. Moreover, the eBOSS-like density mock catalog ($N_{voids} = 5728$) presents the lowest signal-to-noise, $S/N = 5.6$. We see that the reconstruction of the voids always improves with more QSOs density and the S/N rises.

With this information, the best result of the different mock catalogs comes from the J-PAS high density, because it presents the highest S/N and κ signal. This high S/N means promising cosmological studies with the J-PAS survey, because the J-PAS high density catalog that we created is a conservative estimate of the actual QSO density to be produced by J-PAS. Consequently, the future QSOs catalog can be even better.

4.4 J-PAS high density mock catalog

4.4.1 Stacked κ profile with photo-z error

Previously, we neglected the effects of the realtively small photo-z errors from J-PAS survey and we used the true redshifts in Websky to find voids and estimate the S/N. However, to account for this imperfection due to the photo-z, we tested what happens when a Gaussian photo-z scatter is added to model the baseline J-PAS expectations.

The photo-z for a given source is expressed by $\triangle z = (z_{phot} - z_{spec})/(1 + z_{spec})$, we can approximate that following a Gaussian distribution. Moreover, the filter system of the J-PAS instrument, described at Section 2.1, was designed to extract photo-z's of the Luminous Red Galaxies (LRG) with accuracy as $\sigma_z \approx 0.003(1 + z)$. Of course, this filter configuration is also ideal to detect and extract photo-z's of type-I quasars. In [60], it has been studied the photo-z error in the future observation of quasars data of the J-PAS survey. It concludes that with a narrow-band filter system, the error of the photometric redshift can be lower than $\sigma_z \approx 0.002(1 + z)$. With this information, we want to study how this error will affect the stacked κ signal of the cosmic voids in the future observational data of the J-PAS survey.

We implemented the photo-z error in the J-PAS high mock catalog with $\sigma = 30$ Mpc/h and $\delta_{min} = -0.2$. As we can see in 18, the stacked lensing profile of the cosmic voids and the signal-to-noise, $S/N = 7.4$, has a subtle increase if we consider the photo-z error. Moreover, we notice there is a decrease of ≈ 500 cosmic voids in one octant considering the σ_z.

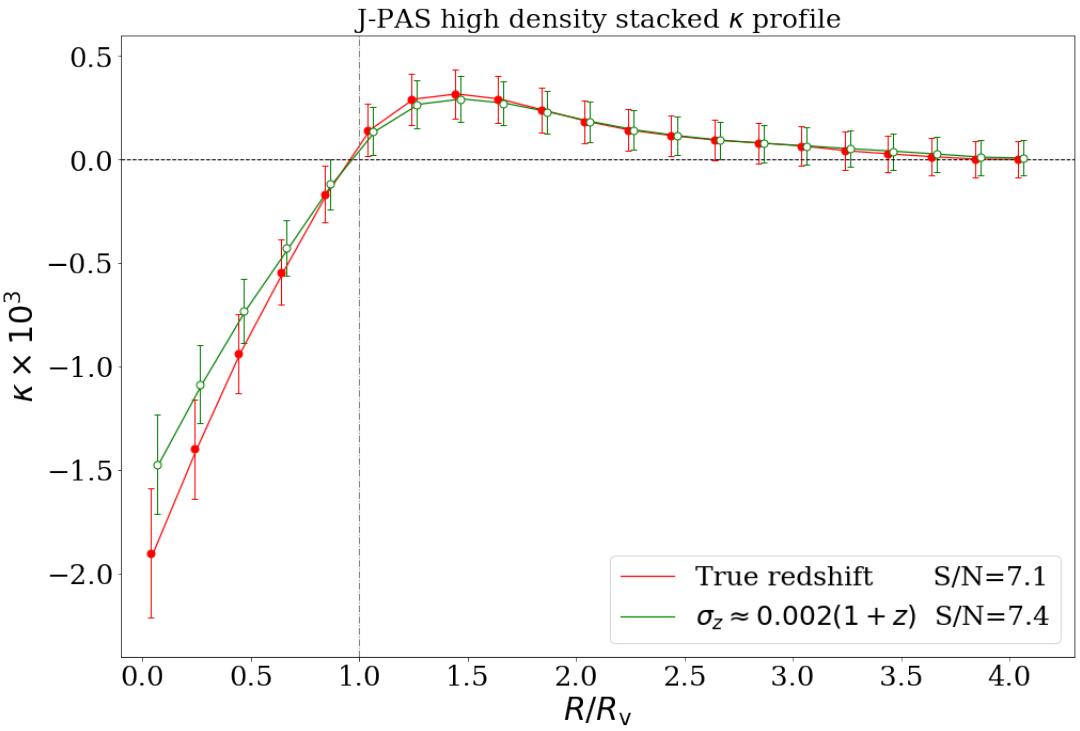

Figure 18: Stacked CMB κ signal + error bars from 1000 random simulations of the J-PAS high mock catalog. *Blue profile:* It is shown the effect of the photo-z error resulting in a slight increase of the κ signal and S/N.

4.4.2 Stacked κ profile up to $z < 2.8$

We focused our study in finding cosmic voids, using quasars at $0.8 < z < 2.2$ to compare with more accuracy the J-PAS survey with eBOSS survey. However, J-PAS survey will provide data of more than 3 million QSOs, up to ≈ 6. In our mock catalog we can only increase the redshift to $z < 2.8$, because if we go to higher redshifts the QSO data is too sparse and the algorithm does not find any consistent voids. In this section we study what happens to the κ profile if we consider larger redshifts than $0.8 < z < 2.2$.

From the $2.2 < z < 2.8$, the 2D void finder found 21640 cosmic voids, presenting a S/N = 2.8 (as shown in the Figure 19). The κ signal is reduced compared to the baseline sample, due to the already falling number density of the QSOs at these higher redshifts. Formally, as shown in Figure 19, this also reduces the overall κ signal at $0.8 < z < 2.2$. The overall $S/N = 7.4$ is slightly better, but is still very close, indicating that the contribution of the $2.2 < z < 2.8$ to the S/N is very low.

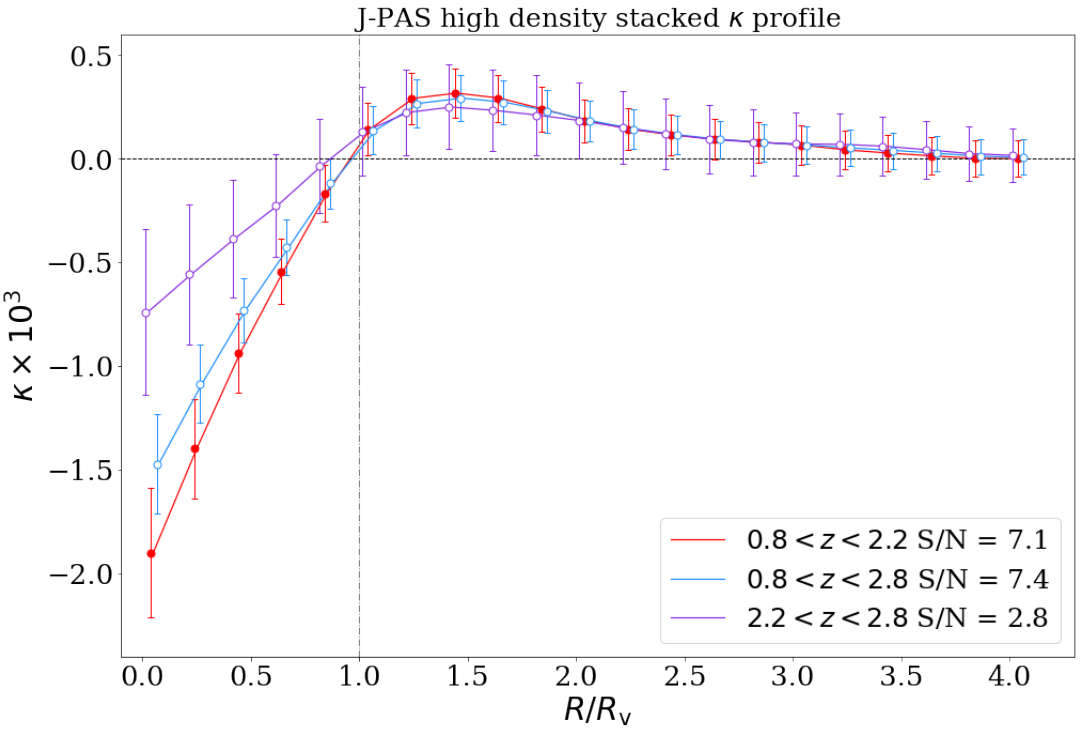

Figure 19: Stacked CMB κ signal of the J-PAS high mock catalog with a grow of the redshift range $z > 2$. The contribution of the $2.2 < z < 2.8$ to the overall $0.8 < z < 2.8$ signal-to-noise is very low, and by adding a lot of voids the κ signal drops a bit due to the less *perfect* voids.

We concluded that the best parameter setting was using a $\sigma = 30$ Mpc/h but in most of the studies ([58] and [32]) it is normally used a lower σ value. We can only consider this smaller smoothing to the highest QSOs density field (J-PAS high), because a too small smoothing in a sparse tracer fields can also result in the detection of spurious voids. Therefore, using the same methodology, we compare the baseline catalog with a stacked κ profile using $\sigma = 20$ Mpc/h. As shown in Figure 20, the resulting signal-to-noise with $\sigma = 20$ Mpc/h increases up to $S/N = 9.4$, whereas the stacked κ does not present a bigger difference.

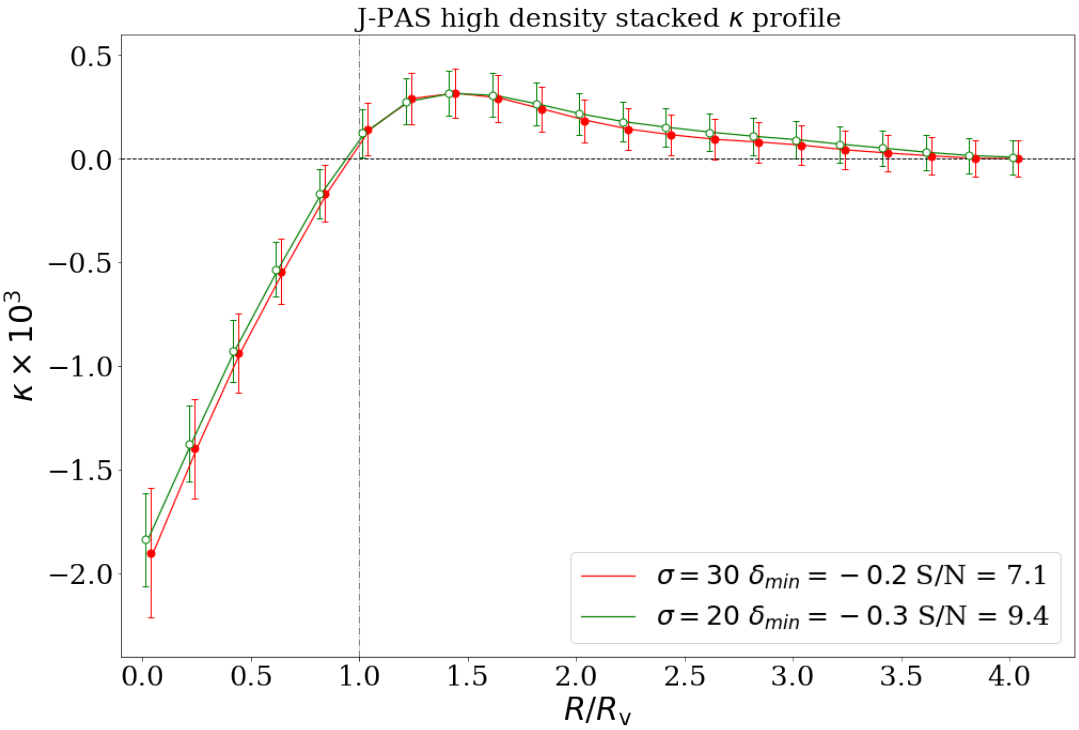

Figure 20: Stacked CMB κ signal of the J-PAS high mock catalog using a lower smoothing scale.

5 Conclusions and discussion

The aim of this project was to explore the prospects of J-PAS cosmic voids cross-correlation with diverse CMB secondary effects (ISW, SZ and lensing), in order to access to more additional cosmological information than using traditional probes (galaxy clustering, BAO, etc). In particular, we focused on the CMB lensing forecast analysis because it is the most promising observable given the redshift range ($0.8 < z < 2.2$) of the QSOs tracer catalogs. Our procedure was to first determine what a current eBOSS-like survey could reveal with the stacked CMB κ signal of cosmic voids, creating a QSO mock catalog with the public Websky simulations. With this starting point, we raised the number density of QSOs in two steps, $1.5x$ (J-PAS low) and $2x$ (J-PAS high), to see how much J-PAS could improve it. We conclude that the optimal parameters in our samples are $\sigma = 30$ Mpc/h and $\delta_{min} = -0.2$, to achieve a higher κ signal, and a larger number of voids.

We robustly determined that J-PAS survey will have a better constraining power than eBOSS. While the J-PAS low mock catalog features a lower signal-to-noise $S/N = 6.5$, J-PAS high presented the highest, $S/N = 7.1$, formally meaning an approximately 20% increase in S/N compared to the eBOSS-like QSO mock. We observe that a higher tracer density produces a better S/N. This happens because when the tracer density is small, the reconstruction of the voids is imperfect and the corresponding κ signal is weaker (less negative). Moreover, if we compare the number of voids of these three mock catalogs, we notice that J-PAS high catalog presents 37449 of voids while an eBOSS-like catalog has a higher number, $N_{voids} = 45818$. We suppose that eBOSS produces more detections of spurious voids, because a lower tracer density field has more empty spaces in the sky,

that the 2D void finder recognizes as cosmic voids.

We also tested the effect of the photo-z error ($\sigma_z \approx 0.002(1+z)$ [60]) using the J-PAS high mock catalog as baseline. We wanted to see how this presumably small photo-z error would affect the study of the CMB κ signal of cosmic voids in the J-PAS QSO catalog. We found that with the photo-z error the number of voids decreases in 10% and the differences between the S/N and the κ signal of the stacked voids do not change significantly, there is only a subtle increase. A possible explanation of the increased signal is that the 500 voids that were lost are spurious voids, which disappeared after slightly perturbing the cosmic web positions of the QSO with the photo-z error, and the remaining voids are more robust. Moreover, the results of the number of voids are consistent with [32], where they analyze the relative number of spec-z (*True redshift*) and photo-z (with σ_z) voids modelling a galaxy sample of DES-SV. They found that photo-z samples present less voids, with the difference being more important for small voids and presenting an almost exact match in the void position and radius for voids substantially larger than the photo-z dispersion.

To explore further options beyond the planned analysis, we evaluated the impact in the κ profile if we increased the redshift range ($0.8 < z < 2.8$), because J-PAS survey will observe up to large redshift quasars. The contribution of the QSO mock catalog at $2.2 < z < 2.8$,drops the κ signal to the overall $0.8 < z < 2.8$ and also, contributes slightly to increase the $S/N = 7.4$, even though it increases by an $\approx 35\%$ the number of voids. This is because the data at this redshift range are very sparse, and the void reconstruction is less perfect. Moreover, the values of the S/N are not directly additive.

At the end of this project, we focused our analysis using J-PAS high with a lower smoothing scale $\sigma = 20$ Mpc/h. We implemented the same methodology to calculate the signal-to-noise. It presents a significant increase of the $S/N = 9.4$ and a 55% more of number of voids than in J-PAS-high, with a similar κ profile. It seems to work with the J-PAS high mock catalog, but also the presence of the spurious voids is high. It is comforting to know that we will be able to produce the κ signal with a higher S/N and perform better analysis of cosmic voids using the future catalogs with a higher QSOs density.

In this work we probed, with simulated QSOs data, that J-PAS survey will have a better constraining power than eBOSS studying the κ signal from cosmic voids. To expand this project in the future, it would be interesting to compare our results with the observational data, when the QSO catalog from J-PAS is finished. Moreover, we can apply the same methodology to study the other CMB maps and use the overall information to probe the ΛCDM model and study the nature of dark energy.

References

[1] Albert, E., Perrett, W., Jeffery, G. (1916).

The foundation of the general theory of relativity.

Ann. Der Phys, 49, 769-822.Link

[2] Aubert, M., Cousinou, M. C., Escoffier, S., Hawken, A. J., Nadathur, S., Alam, S., ... Zhao, C. (2022).

The completed SDSS-IV extended Baryon Oscillation Spectroscopic Survey: growth rate of structure measurement from cosmic voids.

Monthly Notices of the Royal Astronomical Society, 513(1), 186-203. Link

[3] Shandarin, S. F. (2011).

The multi-stream flows and the dynamics of the cosmic web.

Journal of Cosmology and Astroparticle Physics, 2011(05), 015. Link

[4] Hamaus, N., Aubert, M., Pisani, A., Contarini, S., Verza, G., Cousinou, M. C., ... Romelli, E. (2022).

Euclid: Forecasts from redshift-space distortions and the Alcock–Paczynski test with cosmic voids.

Astronomy Astrophysics, 658, A20.Link

[5] Bonici, M., Carbone, C., Vielzeuf, P., Paganin, L., Cardone, V., Hamaus, N., ... Andreon, S. (2022).

Euclid: Forecasts from the void-lensing cross-correlation.

arXiv preprint arXiv:2206.14211.Link

[6] Hamaus, N., Pisani, A., Sutter, P. M., Lavaux, G., Escoffier, S., Wandelt, B. D., Weller, J. (2016).

Constraints on Cosmology and Gravity from the Dynamics of Voids.

Physical Review Letters, 117(9), 091302. Link

[7] Riess, A. G., Filippenko, A. V., Challis, P., Clocchiatti, A., Diercks, A., Garnavich, P. M., ... Tonry, J. (1998).

Observational evidence from supernovae for an accelerating universe and a cosmological constant.

The Astronomical Journal, 116(3), 1009. Link

[8] Mao, Q., Berlind, A. A., Scherrer, R. J., Neyrinck, M. C., Scoccimarro, R., Tinker, J. L., ... Malanushenko, V. (2017).

A cosmic void catalog of SDSS DR12 BOSS galaxies.

The Astrophysical Journal, 835(2), 161. Link

[9] Perlmutter, S., Aldering, G., Goldhaber, G., Knop, R. A., Nugent, P., Castro, P. G., ... Supernova Cosmology Project. (1999).

Measurements of and from 42 high-redshift supernovae.

The Astrophysical Journal, 517(2), 565. Link

[10] Perivolaropoulos, L., Skara, F. (2022).

Challenges for CDM: An update.

New Astronomy Reviews, 101659. Link

[11] Penzias, A. A., Wilson, R. W. (1965).

A measurement of excess antenna temperature at 4080 Mc/s.

The Astrophysical Journal, 142, 419-421. Link

[12] Collaboration, P., Aghanim, N., Akrami, Y., Ashdown, M., Aumont, J., Baccigalupi, C., ... Rosset, C. (2020).

Planck 2018 results. VI. Cosmological parameters. Link

[13] Bond, J. R., Kofman, L., Pogosyan, D. (1996).

How filaments of galaxies are woven into the cosmic web.

Nature, 380(6575), 603-606. Link

[14] Colless, M., Peterson, B. A., Jackson, C., Peacock, J. A., Cole, S., Norberg, P., ... Taylor, K. (2003).

The 2dF galaxy redshift survey: final data release.

arXiv preprint astro-ph/0306581.Link

[15] Tamone, A., Zhao, C., Forero-Sánchez, D., Variu, A., Chuang, C. H., Kitaura, F. S., ... Tao, C. (2022).

Void BAO measurements on quasars from eBOSS.

arXiv preprint arXiv:2208.06238. Link

[16] Hawken, A. J., Aubert, M., Pisani, A., Cousinou, M. C., Escoffier, S., Nadathur, S., ... Schneider, D. P. (2020).

Constraints on the growth of structure around cosmic voids in eBOSS DR14.

Journal of Cosmology and Astroparticle Physics, 2020(06), 012. Link

[17] Tegmark, M., Blanton, M. R., Strauss, M. A., Hoyle, F., Schlegel, D., Scoccimarro, R., ... SDSS Collaboration. (2004).

The three-dimensional power spectrum of galaxies from the sloan digital sky survey.

The Astrophysical Journal, 606(2), 702. Link

[18] Pieri, M. M., Bonoli, S., Chaves-Montero, J., Pâris, I., Fumagalli, M., Bolton, J. S., ... Collaboration, T. W. (2016).

WEAVE-QSO: a massive intergalactic medium survey for the william herschel telescope.

arXiv preprint arXiv:1611.09388. Link

[19] Huchra, J., Jarrett, T., Skrutskie, M., Cutri, R., Schneider, S., Macri, L., ... George, T. (2005, June).

The 2mass redshift survey and low galactic latitude large-scale structure. In Nearby Large-Scale Structures and the Zone of Avoidance Link

[20] Kovács, A., Jeffrey, N., Gatti, M., Chang, C., Whiteway, L., Hamaus, N., ... Weller, J. (2022).

The DES view of the Eridanus supervoid and the CMB cold spot.

Monthly Notices of the Royal Astronomical Society, 510(1), 216-229. Link

[21] Kreisch, C. D., Pisani, A., Carbone, C., Liu, J., Hawken, A. J., Massara, E., ... Wandelt, B. D. (1877).

Massive neutrinos leave fingerprints on cosmic voids.

Monthly Notices of the Royal Astronomical Society.Link

[22] Weygaert, R., Kreckel, K., Platen, E., Beygu, B., Van Gorkom, J. H., van der Hulst, J. M., ... Yip, C. W. (2011).

The void galaxy survey. In Environment and the Formation of Galaxies: 30 years later (pp. 17-24). Springer, Berlin, Heidelberg. Link

[23] Kovács, A., Vielzeuf, P., Ferrero, I., Fosalba, P., Demirbozan, U., Miquel, R., ... Weller, J. (2022).

Dark Energy Survey Year 3 results: imprints of cosmic voids and superclusters in the Planck CMB lensing map.

Monthly Notices of the Royal Astronomical Society, 515(3), 4417-4429.Link

[24] Nelson, D., Springel, V., Pillepich, A., Rodriguez-Gomez, V., Torrey, P., Genel, S., ... Hernquist, L. (2019).

The IllustrisTNG simulations: public data release.

Computational Astrophysics and Cosmology, 6(1), 1-29. Link

[25] Davé, R., Anglés-Alcázar, D., Narayanan, D., Li, Q., Rafieferantsoa, M. H., Appleby, S. (2019).

SIMBA: Cosmological simulations with black hole growth and feedback.

Monthly Notices of the Royal Astronomical Society, 486(2), 2827-2849. Link

[26] Sehgal, N., Bode, P., Das, S., Hernandez-Monteagudo, C., Huffenberger, K., Lin, Y. T., ... Trac, H. (2010).

Simulations of the microwave sky.

The Astrophysical Journal, 709(2), 920.Link

[27] Battaglia, N., Bond, J. R., Pfrommer, C., Sievers, J. L. (2012).

ON THE CLUSTER PHYSICS OF SUNYAEV–ZEL'DOVICH AND X-RAY SURVEYS. II. DECONSTRUCTING THE THERMAL SZ POWER SPECTRUM.

The Astrophysical Journal, 758(2), 75. Link

[28] Granett, B. R., Neyrinck, M. C., Szapudi, I. (2008).

An imprint of superstructures on the microwave background due to the integrated Sachs-Wolfe effect.

The Astrophysical Journal, 683(2), L99. Link

[29] Kovács, A., Sánchez, C., García-Bellido, J., Elvin-Poole, J., Hamaus, N., Miranda, V., ... DES Collaboration. (2019).

More out of less: an excess integrated Sachs–Wolfe signal from supervoids mapped out by the Dark Energy Survey.

Monthly Notices of the Royal Astronomical Society, 484(4), 5267-5277. Link

[30] Alonso, D., Hill, J. C., Hložek, R., Spergel, D. N. (2018).

Measurement of the thermal Sunyaev-Zel'dovich effect around cosmic voids.

Physical Review D, 97(6), 063514. Link

[31] Nozawa, S., Itoh, N., Suda, Y., Ohhata, Y. (2005).

An improved formula for the relativistic corrections to the kinematical Sunyaev-Zeldovich effect for clusters of galaxies.

arXiv preprint astro-ph/0507466.Link

[32] Sánchez, C., Clampitt, J., Kovacs, A., Jain, B., García-Bellido, J., Nadathur, S., ... DES Collaboration. (2016).

Cosmic voids and void lensing in the Dark Energy Survey Science Verification data.

Monthly Notices of the Royal Astronomical Society, stw2745. Link

[33] Metcalf, R. B., Meneghetti, M. A. S. S. I. M. O., Avestruz, C., Bellagamba, F., Bom, C. R., Bertin, E., ... Vernardos, G. (2019).

The strong gravitational lens finding challenge.

Astronomy Astrophysics, 625, A119. Link

[34] Hang, Q., Alam, S., Cai, Y. C., Peacock, J. A. (2021).

Stacked CMB lensing and ISW signals around superstructures in the DESI Legacy Survey.

Monthly Notices of the Royal Astronomical Society, 507(1), 510-523. Link

[35] Stein, G., Alvarez, M. A., Bond, J. R. (2019).

The mass-Peak Patch algorithm for fast generation of deep all-sky dark matter halo catalogues and its N-body validation.

Monthly Notices of the Royal Astronomical Society, 483(2), 2236-2250.Link

[36] Bonici, M., Carbone, C., Vielzeuf, P., Paganin, L., Cardone, V., Hamaus, N., ... Andreon, S. (2022).

Euclid: Forecasts from the void-lensing cross-correlation.

arXiv preprint arXiv:2206.14211. Link

[37] Hamaus, N., Aubert, M., Pisani, A., Contarini, S., Verza, G., Cousinou, M. C., ... Romelli, E. (2022).

Euclid: Forecasts from redshift-space distortions and the Alcock–Paczynski test with cosmic voids.

Astronomy Astrophysics, 658, A20. Link

[38] Mandelbaum, R., Blazek, J., Chisari, N. E., Collett, T., Galbany, L., Gawiser, E., ... Sullivan, M. (2019).

Wide-field multi-object spectroscopy to enhance dark energy science from LSST.

arXiv preprint arXiv:1903.09323. Link

[39] Alarcon, A., Gaztanaga, E., Eriksen, M., Baugh, C. M., Cabayol, L., Casas, R., ... Tallada-Crespí, P. (2021).

The PAU Survey: an improved photo-z sample in the COSMOS field.

Monthly Notices of the Royal Astronomical Society, 501(4), 6103-6122. Link

[40] Lima, E. V. R., Sodré Jr, L., Bom, C. R., Teixeira, G. S., Nakazono, L., Buzzo, M. L., ... Schoennell, W. (2022).

Photometric redshifts for the S-PLUS Survey: Is machine learning up to the task?.

Astronomy and Computing, 38, 100510. Link

[41] Kovács, A., Beck, R., Smith, A., Rácz, G., Csabai, I., Szapudi, I. (2022).

Evidence for a high-z ISW signal from supervoids in the distribution of eBOSS quasars.

Monthly Notices of the Royal Astronomical Society, 513(1), 15-26. Link

[42] Dark Energy Survey Collaboration. (2005).

The dark energy survey.

arXiv preprint astro-ph/0510346.Link

[43] Benitez, N., Dupke, R., Moles, M., Sodre, L., Cenarro, J., Marin-Franch, A., ... Solano, E. (2014).

J-PAS: the Javalambre-physics of the accelerated universe astrophysical survey.

arXiv preprint arXiv:1403.5237. Link

[44] Bonoli, S., Marín-Franch, A., Varela, J., Ramió, H. V., Abramo, L. R., Cenarro, A. J., ... Vitorelli, A. Z. (2020).

The miniJPAS survey: a preview of the Universe in 56 colours.

arXiv preprint arXiv:2007.01910. Link

[45] Lavaux, G., Wandelt, B. D. (2012).

Precision cosmography with stacked voids.

The Astrophysical Journal, 754(2), 109. Link

[46] Alcock, C., Paczyński, B. (1979).

An evolution free test for non-zero cosmological constant.

Nature, 281(5730), 358-359. Link

[47] Kitayama, T. (2014).

Cosmological and astrophysical implications of the Sunyaev–Zel'dovich effect.

Progress of Theoretical and Experimental Physics, 2014(6). Link

[48] Ade, P. A., Aghanim, N., Arnaud, M., Ashdown, M., Aumont, J., Baccigalupi, C., ... Naselsky, P. (2016).

Planck 2015 results-XV. Gravitational lensing.

Astronomy Astrophysics, 594, A15.Link

[49] Tanimura, H. (2017).

Probing the large-scale structure of the Universe with the Sunyaev-Zel'dovich Effect. Link

[50] Lvo, E. V., SUNYAE, R., ZELDovo, Y. A. B. (1972).

The Induced Light Pressure under Astrophysical Conditions.

Astron. Astrophys, 19, 135-139. Link

[51] Schneider, P. (2006).

Weak gravitational lensing. In Gravitational lensing: strong, weak and micro

Springer, Berlin, Heidelberg. Link

[52] Stein, G., Alvarez, M. A., Bond, J. R., van Engelen, A., Battaglia, N. (2020).

The Websky extragalactic CMB simulations.

Journal of Cosmology and Astroparticle Physics, 2020(10), 012. Link

[53] Ade, P. A. R., Aghanim, N., Arnaud, M., Ashdown, M., Aumont, J., Baccigalupi, C., ... Moss, A. (2016).

Planck 2015 results-XXI. The integrated Sachs-Wolfe effect.

Astronomy Astrophysics, 594, A21. Link

[54] Seljak, U. (1995).

Rees-Sciama effect in a CDM universe.

arXiv preprint astro-ph/9506048.Link

[55] Battaglia, N., Bond, J. R., Pfrommer, C., Sievers, J. L. (2012).

ON THE CLUSTER PHYSICS OF SUNYAEV–ZEL'DOVICH AND X-RAY SURVEYS. II. DECONSTRUCTING THE THERMAL SZ POWER SPECTRUM.

The Astrophysical Journal, 758(2), 75. Link

[56] Trac, H., Bode, P., Ostriker, J. P. (2011).

Templates for the Sunyaev–Zel'dovich angular power spectrum.

The Astrophysical Journal, 727(2), 94. Link

[57] Battaglia, N., Bond, J. R., Pfrommer, C., Sievers, J. L., Sijacki, D. (2010).

SIMULATIONS OF THE SUNYAEV–ZEL'DOVICH POWER SPECTRUM WITH ACTIVE GALACTIC NUCLEUS FEEDBACK.

The Astrophysical Journal, 725(1), 91. Link

[58] Vielzeuf, P., Kovács, A., Demirbozan, U., Fosalba, P., Baxter, E., Hamaus, N., ... DES Collaboration. (2021).

Dark Energy Survey Year 1 results: the lensing imprint of cosmic voids on the cosmic microwave background.

Monthly Notices of the Royal Astronomical Society, 500(1), 464-480. Link

[59] Kovács, A., Sánchez, C., García-Bellido, J., Nadathur, S., Crittenden, R., Gruen, D., ... DES Collaboration). (2017).

Imprint of DES superstructures on the cosmic microwave background.

Monthly Notices of the Royal Astronomical Society, 465(4), 4166-4179.Link

[60] Abramo, L. R., Strauss, M. A., Lima, M., Hernández-Monteagudo, C., Lazkoz, R., Moles, M., ... Storchi-Bergmann, T. (2012).

Measuring large-scale structure with quasars in narrow-band filter surveys.

Monthly Notices of the Royal Astronomical Society, 423(4), 3251-3267. Link